

Peanuts at an Angle: Detecting and Measuring the Three-Dimensional Structure of Bars in Moderately Inclined Galaxies

Peter Erwin^{1,2*} and Victor P. Debattista³

¹*Max-Planck-Institut für extraterrestrische Physik, Giessenbachstrasse, 85748 Garching, Germany*

²*Universitäts-Sternwarte München, Scheinerstrasse 1, D-81679 München, Germany*

³*Jeremiah Horrocks Institute, University of Central Lancashire, Preston PR1 2HE, UK*

11 December 2013

ABSTRACT

We show that direct detection and measurement of the vertically thickened parts of bars (so-called “boxy” or “peanut-shaped” bulges) is possible not only for edge-on galaxies but also for galaxies with moderate inclinations ($i < 70^\circ$), and that examples are relatively common in the nearby Universe.

Analysis of a sample of 78 nearby, moderately inclined ($i \lesssim 65^\circ$) early-type (S0–Sb) barred galaxies shows that the isophotal signature of the box/peanut can usually be detected for inclinations as low as $i \sim 40^\circ$ – and in exceptional cases down to $i \sim 30^\circ$. In agreement with the predictions from N -body simulations, the signature is most easily detectable when the bar’s position angle is within $\sim 50^\circ$ of the galaxy major axis; in particular, galaxies where the bar lies very close to the minor axis do not show the signature clearly or at all. For galaxies with $i = 40$ – 65° and relative angles $< 45^\circ$, we find evidence for the signature $\approx 2/3$ of the time; the true frequency of box/peanut structures in bars may be higher.

Comparison with N -body models also allows us to link observed photometric morphology with 3D physical structures, and thus estimate the relative sizes of box/peanut structures and bars. For our local sample, we find that box/peanut structures range in radial size (measured along the bar major axis) from 0.4–3.8 kpc (mean = 1.5 ± 0.9 kpc) and span 0.26–0.58 of the bar length (mean of 0.38 ± 0.08). This is a clear observational confirmation that when bars thicken, it is not the entire bar which does so, but only the inner part.

This technique can also be used to identify galaxies with bars which have *not* vertically thickened. We suggest that NGC 3049 and IC 676 may be particularly good examples, and that the fraction of S0–Sb bars which *lack* box/peanut structures is at least $\sim 13\%$.

Key words: galaxies: structure – galaxies: elliptical and lenticular, cD – galaxies: spiral – galaxies: evolution.

1 INTRODUCTION

For a long time, the vertically thickened inner regions of disc galaxies have been referred to as “bulges”, for straightforward descriptive reasons. For almost as long, these have been understood to be spheroidal, kinematically hot structures, akin to elliptical galaxies. However, peculiar exceptions have also been known for some time – in particular, cases where bulges seen in edge-on galaxies have a distinctly “boxy” or even “peanut-shaped” morphology. A series of imaging

studies (Jarvis 1986; de Souza & Dos Anjos 1987; Shaw 1987; Dettmar & Barteldrees 1990; Lütticke et al. 2000a) gradually demonstrated that such structures are actually quite common; Lütticke et al. found that $\sim 45\%$ of edge-on bulges in S0–Sd galaxies are boxy or peanut-shaped. Even the Galaxy’s own bulge has turned out to be boxy (e.g., Kent et al. 1991; Dwek et al. 1995). The peculiarity is not just morphological: several early stellar-kinematic studies noted that strongly boxy or peanut-shaped bulges exhibited *cylindrical* stellar rotation (e.g., Bertola & Capaccioli 1977; Kormendy & Illingworth 1982), something not at all characteristic of elliptical galaxies.

* E-mail: erwin@mpe.mpg.de

Although several models have been proposed for boxy or peanut-shaped bulges, such as their being the results of minor mergers (e.g., Binney & Petrou 1985), the most successful explanation has come from investigations of bar formation and evolution. A pioneering 3D N -body study by Combes & Sanders (1981) noted that the bars which formed in their simulation showed “a peanut-shape morphology” when the model was viewed edge-on with the bar perpendicular to the line of sight, an appearance similar to classic peanut-shaped bulges in systems such as NGC 128. In the early 1990s, simulations of galaxy discs clearly showed that a vertically unstable “buckling” phase often followed the formation of a bar (e.g., Combes et al. 1990; Raha et al. 1991); the morphology and cylindrical kinematics of the resulting structure matched observations of boxy and peanut-shaped bulges (see Athanassoula 2005a and Debattista et al. 2006 for reviews). This rapid, asymmetric buckling phase is usually assumed to be driven by a global bending instability (e.g., Merritt & Sellwood 1994). However, alternate formation mechanisms which involve the resonant heating or trapping of stellar orbits have been suggested (Combes et al. 1990; Quillen 2002; Debattista et al. 2006).

Other theoretical studies have investigated the underlying orbital structure which may support this morphology (e.g., Pfenniger 1985; Pfenniger & Friedli 1991; Patsis et al. 2002; Martinez-Valpuesta et al. 2006), explored conditions under which it may be promoted or suppressed (e.g., Berentzen et al. 1998; Athanassoula & Misiriotis 2002; Athanassoula 2005a; Debattista et al. 2006; Wozniak & Michel-Dansac 2009), and even suggested that multiple phases of buckling and vertical growth can take place (Athanassoula 2005b; Martinez-Valpuesta et al. 2006).

Evidence confirming the association of bars with boxy/peanut-shaped (B/P) bulges in real galaxies has come primarily from spectroscopy of edge-on galaxies. The major-axis kinematics of ionized gas (Kuijken & Merrifield 1995; Merrifield & Kuijken 1999; Bureau & Freeman 1999; Veilleux et al. 1999) and stars (Chung & Bureau 2004) in edge-on galaxies with boxy or peanut-shaped bulges displays the characteristic imprint of bars, as predicted by orbital analyses and simulations, both pure N -body (Athanassoula & Bureau 1999; Bureau & Athanassoula 2005) and hydrodynamical (e.g., Athanassoula & Bureau 1999). (Note, however, that the appearance of this feature in gas kinematics requires that the so-called x_2 orbit family be present, which requires that the bar have an inner Lindblad resonance, something not all bars necessarily have.) In addition, near-IR imaging of edge-on systems indicates that B/P bulges are accompanied by larger-scale extensions in the disc of the galaxy, suggestive of the vertically thin outer zones of bars (Lütticke et al. 2000b; Bureau et al. 2006). The frequency of boxy and peanut-shaped bulges is consistent with most barred galaxies having vertically thickened inner regions (Lütticke et al. 2000a).

Finding B/P bulges is relatively easy in edge-on galaxies – provided the features are strong and not overwhelmed by a large classical bulge, *and* that the bar is favorably aligned: i.e., close to perpendicular to the line of sight. (As the bar orientation shifts closer to end-on, the projection of the B/P bulge becomes rounder and thus harder to distinguish from a classical bulge.) However, measuring the characteristics of the rest of the bar – its length, orientation, strength, shape,

etc. – is much more difficult, both due to dust extinction and to the superposition of stellar light from various regions of the disc along the line of sight. This same difficulty in identifying and measuring the “flat”, planar parts of bars also makes it difficult to find examples of galaxies with bars which have *not* buckled. It would clearly be useful if there were a way to identify the B/P structure in face-on bars, or even in bars of moderately inclined galaxies, where the in-plane structure of the bar and disc is still discernable.

One promising approach is the direct detection of stellar-kinematical features associated with B/P bulges in less inclined galaxies, as proposed by Debattista et al. (2005). Méndez-Abreu et al. (2008) demonstrated that this is possible by detecting the kinematic signature of a B/P structure in the low-inclination ($i = 26^\circ$) barred galaxy NGC 98. However, this method is most useful when the galaxy has a very low inclination ($i < 30^\circ$), and it requires high-S/N spectroscopy and expensive allocations of telescope time (e.g., ~ 3 h on 8–10m-class telescopes).

The standard approach for identifying B/P structures from imagery has been to look at very highly inclined or edge-on galaxies; minimum inclinations of $\sim 75^\circ$ or 80° have been suggested (e.g., Jarvis 1986; Shaw et al. 1990). There *have* been isolated reports of B/P structures in images of galaxies which are highly inclined but not actually edge-on (i.e., inclinations ~ 70 – 85°). Buta (1990) noted the peculiar “inner hexagonal zone” of NGC 7020 ($i = 69^\circ$), even going so far as to suggest a possible connection with box/peanut-shaped structures from the simulations of Combes & Sanders (1981). A few years later, Bettoni & Galletta (1994) pointed out the case of NGC 4442 ($i = 72^\circ$), which they explicitly identified as hosting a thickened bar with projected isophotes similar to those of the B/P structure in the N -body simulations of Combes et al. (1990); they also found evidence for cylindrical rotation in the stellar kinematics, similar to that seen in the simulations. Likewise, Quillen et al. (1997) identified the bar of NGC 7582 ($i \sim 70^\circ$) as hosting a peanut-shaped bulge.

More recently, Athanassoula & Beaton (2006) used a relatively deep 2MASS image of M31 ($i = 77^\circ$) to show that it, too, has a boxy bulge embedded within a longer bar (see also Beaton et al. 2007). By comparing isophotes and surface-brightness profiles from cuts parallel to the major axis of the galaxy with isodensity contours and parallel cuts from a selection of N -body simulations, they demonstrated that the morphology of M31 immediately outside its classical bulge was consistent with that of a bar having both a B/P structure and an outer, flatter region seen at high inclination and a slight offset with respect to the galaxy’s major axis. (They also found similarities between M31’s gas kinematics and predictions from gas flow in barred-galaxy simulations.)

In this paper, we demonstrate that there is a consistent set of isophotal features which makes identification of B/P bulges in images of *moderately* inclined ($i < 70^\circ$) galaxies quite possible, and that numerous examples of galaxies with these features exist. We find that B/P structures can be identified in images even when the inclination is as low as $i \sim 30^\circ$.

Throughout this paper, we assume a Hubble constant of $H_0 = 72 \text{ km s}^{-1} \text{ Mpc}^{-1}$.

1.1 A Note on Terminology

In the course of this study, we use the words “box” and “boxy” rather often, in reference to several related phenomena. For clarity, we will use the terms **boxy/peanut-shaped bulge** and **B/P structure** to refer to a specific 3D stellar structure: the vertically thickened inner part of a bar, as discussed above. We will also use the terms **boxy bar** and **box+spurs**: these refer to a 2D morphological feature seen in the isophotes of moderately inclined galaxies. Much of this paper is devoted to demonstrating that the existence of the former (3D) structure explains the presence of the latter (2D) phenomenon in real galaxies.

2 THE VISUAL PHENOMENON: EXAMPLES OF BOXY BARS FROM VARIOUS SOURCES

We begin by discussing a peculiar morphology seen in some moderately inclined galaxies. Figure 1 shows a characteristic example: the SBa galaxy NGC 5377, which has a strong bar with a radial size of $\sim 65''$ and a position angle on the sky of 45° . The inner part of the bar ($r < 30''$) has isophotes which are rather broad and distinctly “boxy” in shape – in this particular case, almost rectangular. At larger radii, the isophotes of the bar appear as narrower projections outside the boxy zone; we term these projections “spurs”. As we will discuss below, these narrower projections are almost always slightly offset from the major axis of the inner isophotes. We call this composite phenomenon the “**box+spurs**” or “**boxy-bar**” morphology; three more examples can be seen in Figure 2. Laurikainen et al. (2011) recently noted the presence of bars with “boxy/peanut/x-shaped structures (B_x)” in a handful of moderately inclined galaxies, including NGC 5377; this is undoubtedly the same thing.

A list of nearby galaxies showing this morphology is given in Table 1. This list – which is not meant to be comprehensive or complete – is based on inspection of a variety of data sources, including the Sloan Digital Sky Survey (Data Release 7; York et al. 2000; Abazajian et al. 2009), as well as images available via NED, including those from Möllenhoff & Heidt (2001), Eskridge et al. (2002), and Knapen et al. (2003). We also identified some candidates by examining published isophotal maps, including those of Jungwiert et al. (1997), Peletier et al. (1999), and Rest et al. (2001). Three galaxies not already in our list were added from the set of non-edge-on galaxies with “ B_x ” classifications in Laurikainen et al. (2011).¹

2.1 Spurs: Leading and Trailing

One of the most striking aspects of the boxy-bar morphology is the existence of the narrow spurs extending beyond the broader boxy region. These spurs are usually *offset* with respect to the major axis of the interior isophotes. This can be seen in Figures 1 and 2. The diagonal grey lines in Figure 2 indicate the major axis of the boxy regions, where the isophotes have the general shape of rounded rectangles; the

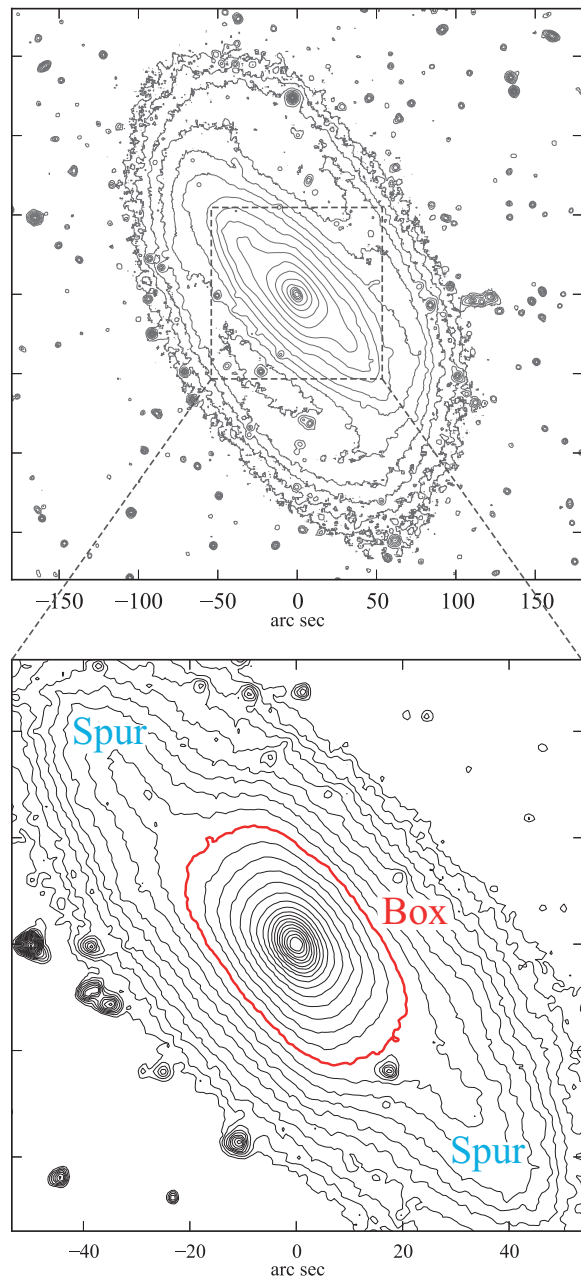


Figure 1. Logarithmically scaled isophotes of the barred Sa galaxy NGC 5377, showing the “boxy-bar”/“box+spurs” morphology. **Top panel:** *R*-band isophotes from Erwin & Sparke (2003); **bottom panel:** close-up of the bar, showing isophotes from an archival *Spitzer* IRAC1 ($3.6\mu\text{m}$) image. The broad, nearly rectangular region in the inner part of the bar is the “box”, labelled in red; the narrow “spurs” projecting outside make up the outer part of the bar and are labelled in blue. In both panels N is up and E is to the left.

narrow spurs extending outside the boxy region are symmetrically offset from this axis.

Could the offset spurs be just an illusion produced by dust? We know that bars often have strong dust lanes running along the leading edges of the bar (e.g., Athanassoula 1992), so in principle offset spurs could be the result of extinction along the bar leading edges. In that case, however,

¹ We exclude NGC 2549, NGC 4220, NGC 5353, and NGC 7332, since they are edge-on, or nearly so.

Table 1. Galaxies with Boxy-Bar Signatures

| Name (1) | Type (2) | Distance (3) | Source (4) | M_B (5) | i (6) | Offset Spurs (7) | Lead/Trail (8) | Source (9) |
|-----------------|--|-----------------|---------------|--------------|------------|---------------------|-------------------|---------------|
| M31 | SA(s)b | 0.79 | 1 | −21.20 | 77 | Yes | trail | 1 |
| NGC 1023 | SB(rs)0 [−] | 11.1 | 3 | −20.94 | 69 | Yes | — | 2 |
| NGC 1079 | (R ₁ R ₂ ')SAB(r'l)a | 17.2 | 4 | −19.11 | 53 | Yes | trail | 2 |
| NGC 1350 | R ₁ 'SB(r)ab | 16.7 | 2 | −20.36 | 57 | Yes | trail | 2 |
| NGC 1375 | SAB0 ⁰ | 31.5 | 3 | −19.39 | 71 | Yes | — | 2 |
| NGC 1415 | (R)SAB0/a(s) | 19.2 | 4 | −19.13 | 65 | Yes | lead | 3 |
| NGC 1784 | SB(r)c | 30.5 | 2 | −21.15 | 52 | Yes | lead | 2 |
| NGC 1808 | (R)SAB(s)a | 12.3 | 2 | −20.17 | 50 | Yes | lead | 2 |
| NGC 2442 | SAB(s)bc pec | 16.2 | 4 | −20.78 | 62 | Yes | lead | 2 |
| NGC 3185 | (R)SB(r)a | 17.5 | 4 | −18.61 | 49 | Yes | lead | 2 |
| NGC 3595 | E? | 33.6 | 4 | −19.89 | 64 | Yes | — | 2 |
| NGC 3627 | SAB(s)b | 10.1 | 5 | −20.92 | 65 | Yes | trail | 2 |
| NGC 3673 | SB(rs)b | 17.4 | 2 | −19.24 | 42 | Yes | lead | 2 |
| NGC 3885 | SA(s)0/a | 23.4 | 4 | −19.57 | 67 | Yes | lead | 2 |
| NGC 3992 | SB(rs)bc | 22.9 | 2 | −22.38 | 56 | Yes | trail | 2 |
| NGC 4123 | SB(r)c | 14.9 | 2 | −19.26 | 45 | Yes | lead | 2 |
| NGC 4192 | SAB(s)ab | 13.6 | 2 | −20.74 | 79 | Yes | trail | 2 |
| NGC 4293 | (R)SB(s)0/a | 16.5 | 6 | −20.35 | 63 | Yes | trail | 4 |
| NGC 4429 | SA(r)0 ⁺ | 16.5 | 6 | −20.20 | 62 | Yes | — | 2,4 |
| NGC 4442 | SB(s)0 ⁰ | 15.3 | 7 | −19.64 | 72 | yes? | — | 5 |
| NGC 4462 | SB(r)ab | 23.9 | 4 | −20.07 | 71 | Yes | trail? | 2 |
| NGC 4535 | SAB(s)c | 15.8 | 5 | −20.62 | 44 | Yes | lead | 2 |
| NGC 4725 | SAB(r)ab pec | 12.4 | 5 | −20.69 | 42 | Yes | trail | 2 |
| NGC 5377 | (R)SB(s)a | 27.1 | 4 | −20.29 | 59 | Yes | trail | 2 |
| NGC 5448 | (R)SAB(r)a | 31.5 | 4 | −20.75 | 66 | Yes | lead | 4 |
| NGC 5641 | (R')SAB(r)ab | 70.2 | 8 | −21.48 | 58 | Yes | trail | 2 |
| NGC 6384 | SAB(r)bc | 25.9 | 2 | −21.52 | 47 | Yes | lead | 2 |
| NGC 7020 | (R)SA(r)0 ⁺ | 40.5 | 4 | −20.56 | 69 | Yes | — | 6 |
| NGC 7582 | R ₁ 'SB(s)ab | 23.0 | 2 | −20.94 | 68 | No? | — | 7 |
| IC 5240 | SB(r)a | 21.8 | 4 | −19.23 | 49 | Yes | lead | 8 |
| ESO 443-39 | S0? | 40.3 | 4 | −19.55 | 57 | Yes | — | 2 |
| UGC 3576 | SB(s)b | 85.0 | 4 | −20.87 | 60 | Yes | trail | 2 |
| UGC 11355 | Sb | 63.1 | 4 | −20.32 | 58 | Yes | — | 2 |

A list of galaxies containing boxy-bar features. This list is not intended to be complete or comprehensive; see Table 2 for examples in a well-defined local sample. (1) Galaxy name; boldface type indicates a particularly strong/emblematic example of the boxy-bar/box+spurs morphology. (2) Hubble type from RC3. (3) Distance in Mpc. (4) Source of distance: 1 = mean of distances in NED; 2 = Tully-Fisher distance from Tully et al. (2009); 3 = SBF distance from Tonry et al. (2001), including metallicity correction from Mei et al. (2005); 4 = HyperLeda redshift (corrected for Virgo-centric infall); 5 = Cepheid distance from Freedman (2001); 6 = mean Virgo Cluster distance from Mei et al. (2007); 7 = SBF distance from Blakeslee et al. (2009); 8 = Tully-Fisher distance from Willick et al. (1997). (5) Absolute B magnitude, from HyperLeda B_{tc} and our adopted distance. (6) Inclination. (7) Indicates whether spurs extending out of boxy zone are offset from major axis of boxy interior. (8) Indicates whether offset spurs, if present, lead or trail (assuming main spiral pattern, if it exists, is trailing). (9) Source of identification: 1 = Athanassoula & Beaton (2006); 2 = this paper; 3 = García-Barreto & Moreno (2000); 4 = Laurikainen et al. (2011); 5 = Bettoni & Galletta (1994); 6 = Buta (1990); 7 = Quillen et al. (1997); 8 = R. Buta, private comm.

we would expect to see only *trailing*-edge spurs, whereas in reality we see both. In fact, we see them with approximately equal frequency: Table 1 has 12 examples of trailing-edge spurs and 13 leading-edge examples. In addition, we see edge spurs in near-IR imaging (e.g., Figures 1 and 2), where dust extinction is weaker or absent, and in S0 galaxies with no detectable gas or dust (e.g., NGC 1023, NGC 3595, NGC 4442, NGC 4429, and ESO 443-39).

Finally, as we will show below (Section 3.1), the N -body models (which are by nature dust-free) have the appearance of spurs as well, and they make a specific prediction about

when the spurs will be offset, and in which direction – a prediction which the observed galaxies match quite well.

3 N -BODY MODELS

We compare observations with a number of collisionless N -body simulations. We rely mainly on three such simulations. The first, run A, has not been previously published. It is a disc galaxy evolving in the prolate halo B described in Debattista et al. (2008). Briefly, this halo was produced by

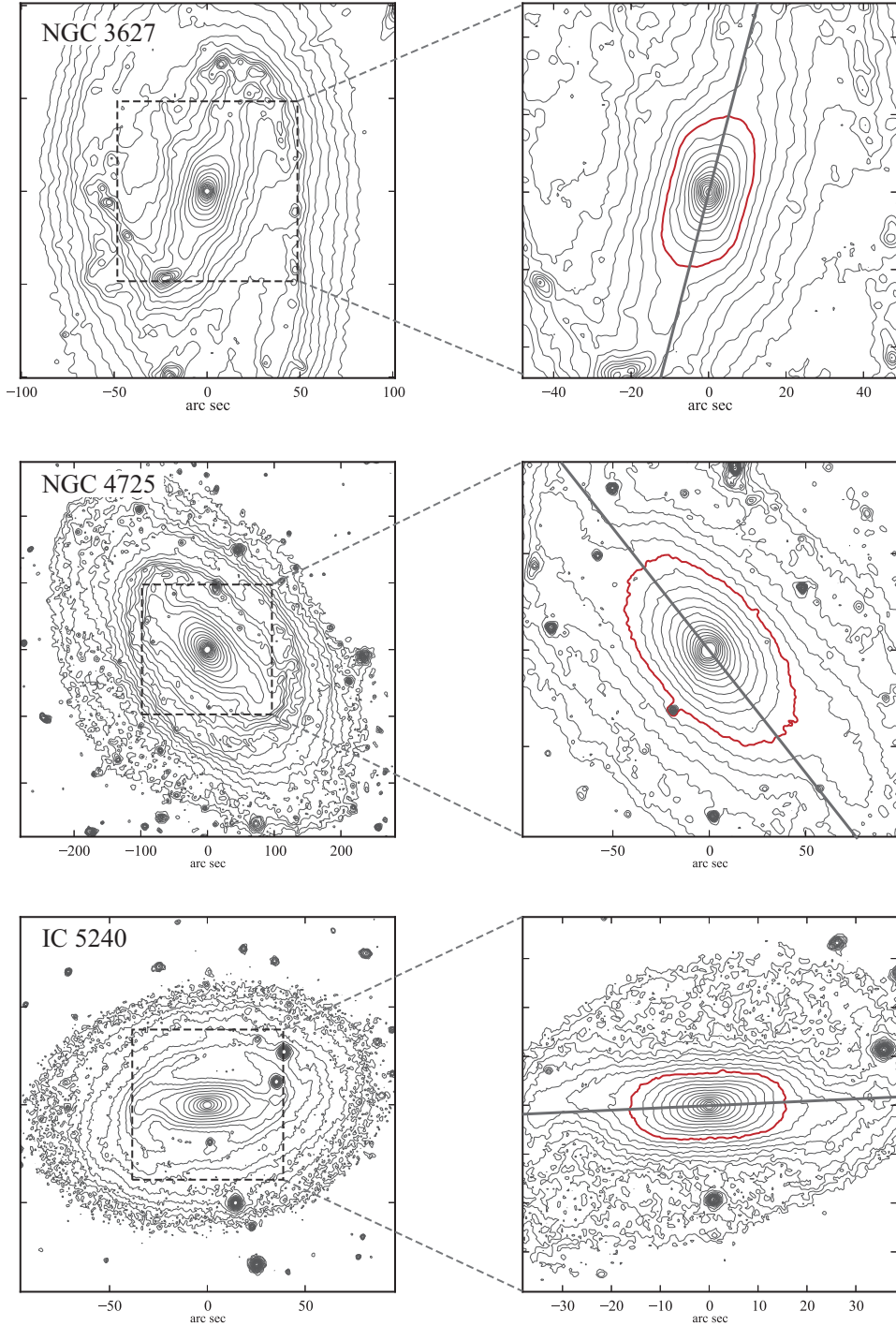


Figure 2. Three more examples of box+spurs morphology in barred galaxies, emphasizing the offset nature of the spurs: NGC 3627 (top, *Spitzer* IRAC1 image from the SINGS project; Kennicutt et al. 2003), NGC 4725 (same image source), and IC 5240 (bottom; left-hand panel is *R*-band image from Koopmann & Kenney (2006), right-hand panel is *K*-band image from Mulchaey et al. (1997)). Dark grey lines in right-hand panels indicate approximate position angle of the boxy regions (outlined with thicker red contour lines); note that the spurs just outside this region are displaced with respect to the lines. Comparison with spiral arms indicates that the spurs are “trailing-edge” in the case of NGC 3627 and NGC 4725, but “leading-edge” in IC 5240. N is up and E is to the left in all panels.

the merger of two spherical haloes starting at rest, 800 kpc apart. The disc grown in this model was exponential with a scale-length of 6 kpc, a Gaussian scale-height $z_d = 300$ pc, a mass of $7 \times 10^{10} M_\odot$ and Toomre $Q = 1.5$. The initial disc is oriented with its angular momentum perpendicular to the

short axis of the (initial) halo, where it remains throughout the simulation. The simulation was evolved with PKDGRAV, as described in Debattista et al. (2008).

The other two models, runs B and C, have already been published in Sellwood & Debattista (2009). These are simu-

lations which differ only in the seed of the random number generator, which was used to set up the initial conditions. Although the two simulations represent instances of the same system, they evolve very differently as a result of the physically very stochastic nature of disc galaxies. The bar amplitude evolution of these two models can be seen in Figure 5 of Sellwood & Debattista: run C is largely growing in strength throughout the simulation and ends in the cluster of lines at the highest amplitude, while run B is strongly weakened by buckling before it starts growing in strength again; this is the simulation with bar amplitude intermediate between the strongest and weakest cases. Further details of these simulations, including a discussion of the importance of stochastic effects, can be found in Sellwood & Debattista. For run B, we use snapshots at $t = 200$ (in simulation units), which is shortly after the bar forms but before it buckles, and at $t = 1000$ (at the end of the simulation, after buckling and a period of bar growth). For run C we use outputs at $t = 200$ (also before buckling) and at $t = 600$ (after the bar has recovered from buckling, with a bar amplitude $A_2 \sim 16\%$ larger than for B at $t = 1000$).

3.1 The 3D Origins of Boxes and Spurs

So what is the origin of the box+spurs morphology? Put simply, it is the result of viewing a bar which has a vertically thick inner region (the B/P structure) and a vertically thin outer region. At moderate to high inclinations, the projection of the B/P structure forms the box, and the vertically thin outer bar forms the spurs. This insight is a generalization of previous work by Bettoni & Galletta (1994) and Athanassoula & Beaton (2006), who compared projections of highly inclined N -body models with single galaxies to come to similar conclusions.²

To demonstrate this, Figure 3 contrasts two different N -body simulations of barred galaxies. On the left is run A, where the bar has buckled and formed a distinct B/P structure, which can be seen in the bottom left, edge-on panels. When seen at intermediate inclinations – and in particular, when seen with the bar at an intermediate angle ΔPA with respect to the line of nodes – the box+spurs morphology emerges; this can be seen most clearly in the $i = 60^\circ$, $\Delta PA = 30^\circ$ panel. In contrast, the right-hand panels show a bar which has *not* buckled. The views of this simulation at moderate inclinations do not show a boxy-bar signature, even in the most favorable $i = 60^\circ$, $\Delta PA = 30^\circ$ view.

In Figure 4, we can see that the *offset* nature of the spurs, pointed out in Section 2.1 for real galaxies, is in the following sense: the spurs are shifted *away* from the major axis, relative to the boxy inner zone. This is because the projection of the B/P structure creates boxy-zone isophotes which are tilted closer to the line of nodes than are the isophotes due to the projection of the outer, flat part of the bar, which form the spurs. (Another way to view this is that when inclination shrinks the observed angle between the outer, flat part of the bar and the line of nodes, it shrinks the apparent angle between the inner part of the bar and the line of nodes *more*, making the boxy zone appear more

closely aligned with the line of nodes than the outer part of the bar.)

Is this consistent with what we see in real galaxies? Of the 35 galaxies where we have been able to directly measure the position angle of the line of nodes and the boxy region (see Table 3 and the figures in the Appendix), we find perfect agreement for all 24 galaxies where the position angles of the line of nodes and the boxy region differ by $\geq 5^\circ$. At smaller relative position angles, we become vulnerable to errors in determining the line of nodes, so that the sense of which direction the box is rotated relative to the line of nodes becomes uncertain. None the less, for the eight galaxies in which the relative angle between box and line of nodes is between 1° and 5° , six show the spurs offset in the correct direction. (Three more galaxies have box and line of nodes position angles differing by $< 1^\circ$, making it effectively impossible to determine the sense in which the box is rotated relative to the line of nodes.)

The correspondence between bar position angle and spur offset shown by both simulated and real galaxies helps rule out other possible explanations for the spurs. For example, in some galaxies the spurs appear to blend smoothly into spiral arms which trail off the ends of the bar – e.g., NGC 3627 and NGC 4725 in Figure 2; this might suggest that the spurs are somehow part of the spiral arms, rather than the outer part of the bar. Inspection of Figure 4 shows that projection effects create the appearance of spiral twisting at the ends of the simulated bars – but the direction of the twist depends on the bar orientation, so that the twisting is always *towards* the line of nodes (compare the far-left and far-right panels). Inspection of the galaxies in Table 1, along with galaxies from our local sample with the boxy-bar morphology (Section 4), reveals nineteen galaxies where the spurs show signs of curvature; in sixteen of these, the curvature is toward the line of nodes, which suggests that this may indeed be an additional projection effect. Given that face-on bars often (in both real galaxy and simulations) appear to have spiral arms trailing off of the ends of bars, we should not be surprised to see spurs blend into spiral arms at larger radii; this does not, however, mean that the entirety of the spur *is* a spiral arm.³

Figure 5 shows a set of projections of one N -body simulation, arranged by inclination and by the relative position angle of the bar with respect to the line of nodes. We can clearly see that the box/peanut structure becomes more visible as the inclination is increased, which is not surprising (see also Figure 3); what *is* perhaps surprising is that the signature of the projected box/peanut is visible when the inclination is relatively low: it is clearly present for $i = 60^\circ$, and also present when $i = 45^\circ$ and ΔPA is $\sim 30^\circ$. In fact, we can see weak traces of the signature in the $i = 30^\circ$, $\Delta PA = 30^\circ$ panel (i.e., the fact that the main axis of the outer part of the bar appears slightly offset on opposite sides of the centre).

By looking at the full set of projections, we can also see that other, related morphologies are indicators of projected

² In the case of M31, Athanassoula & Beaton’s “elongations” correspond to what we call spurs.

³ For NGC 3627 (Figure 2), we see curvature of the northern spur towards the major axis, which then gives way at larger radii to a spiral arm twisting the *opposite* direction, which strongly argues that the spur is not an inward continuation of the spiral arm.

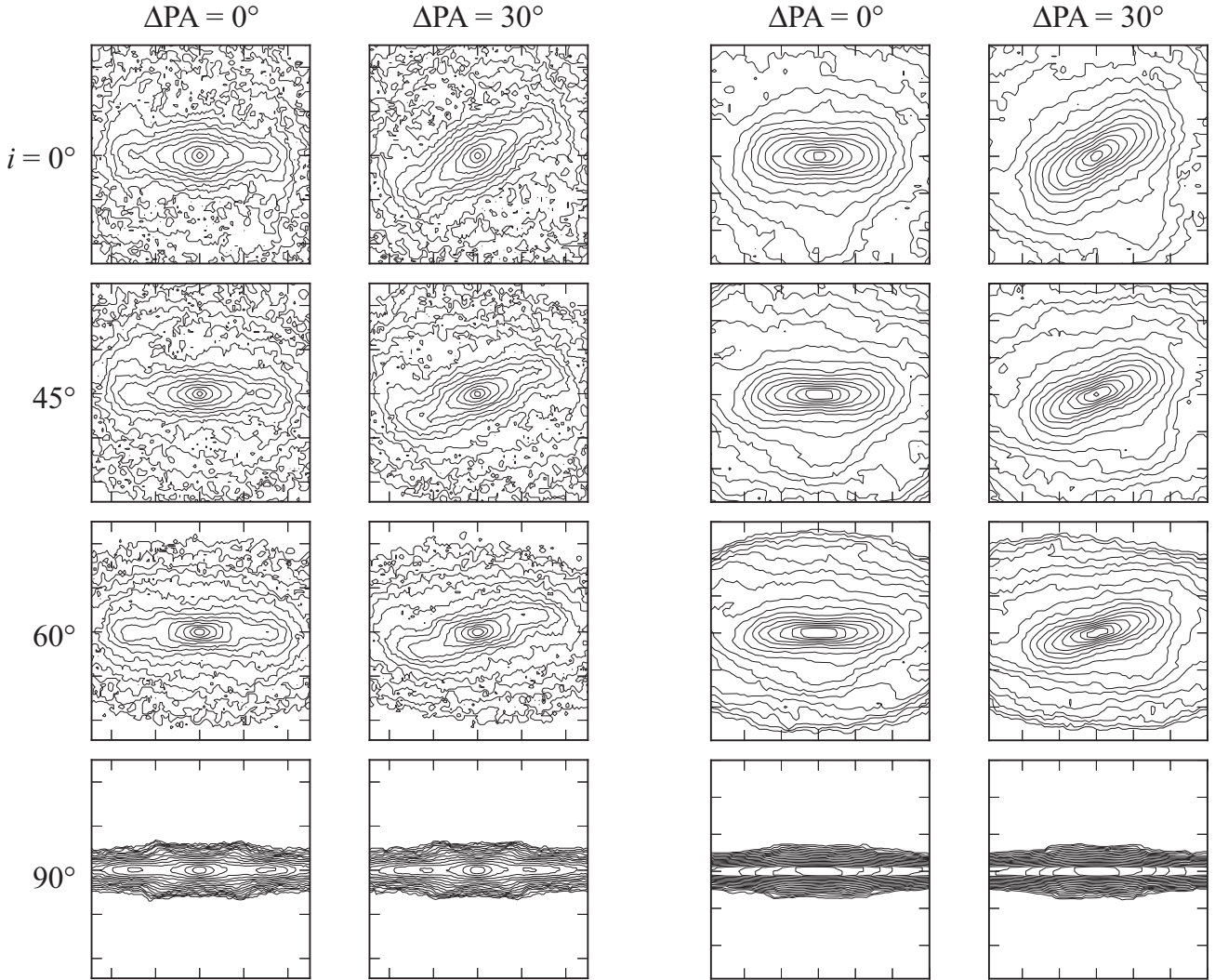


Figure 3. Demonstration that B/P structures in N -body simulations produce the boxy-bar (box+spurs) morphology. **Left panels:** log-scaled isodensity contours of run A, viewed at different inclinations (face-on to edge-on, top to bottom) and with different in-plane angles between bar and line of nodes ($\Delta PA = PA_{\text{bar}} - PA_{\text{disc}}$, measured in the galaxy plane); disc line of nodes is horizontal in all panels. When the simulation is edge-on ($i = 90^\circ$), the peanut-shaped bulge is visible; at lower inclinations (60° and 45°), this projects to form the box of the boxy-bar morphology, while the vertically thin outer part of the bar projects to form the spurs. **Right panels:** same, but showing run B at $t = 200$, where a B/P structure is *not* present; consequently, no box+spurs morphology is seen when the galaxy is moderately inclined.

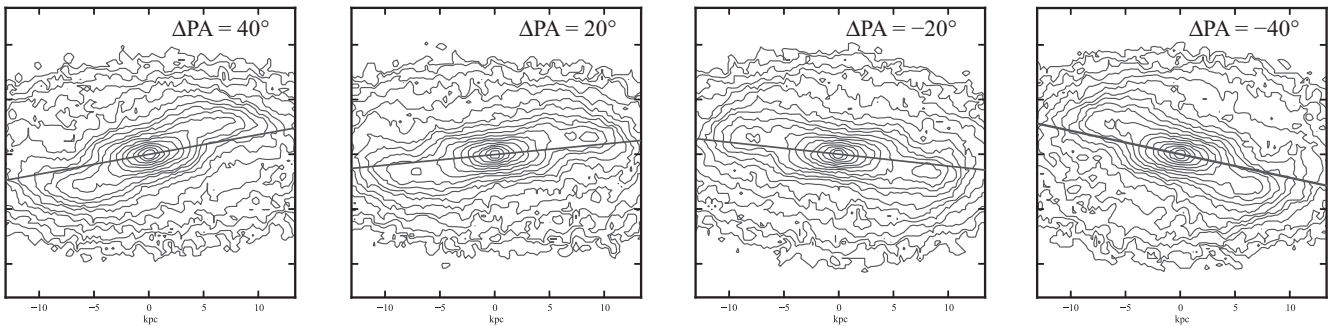


Figure 4. N -body model A, viewed at $i = 60^\circ$. Each panel shows a different rotation of the bar relative to the line of nodes, which is horizontal in all panels: from left to right, $\Delta PA = 40^\circ, 20^\circ, -20^\circ$, and -40° (all measured in the galaxy plane). The dark grey diagonal lines indicate the approximate position angle of the boxy regions; the spurs are displaced with respect to these lines as in Figure 2. The sense of the displacement is always the same: rotated further away from the line of nodes than the boxy region is.

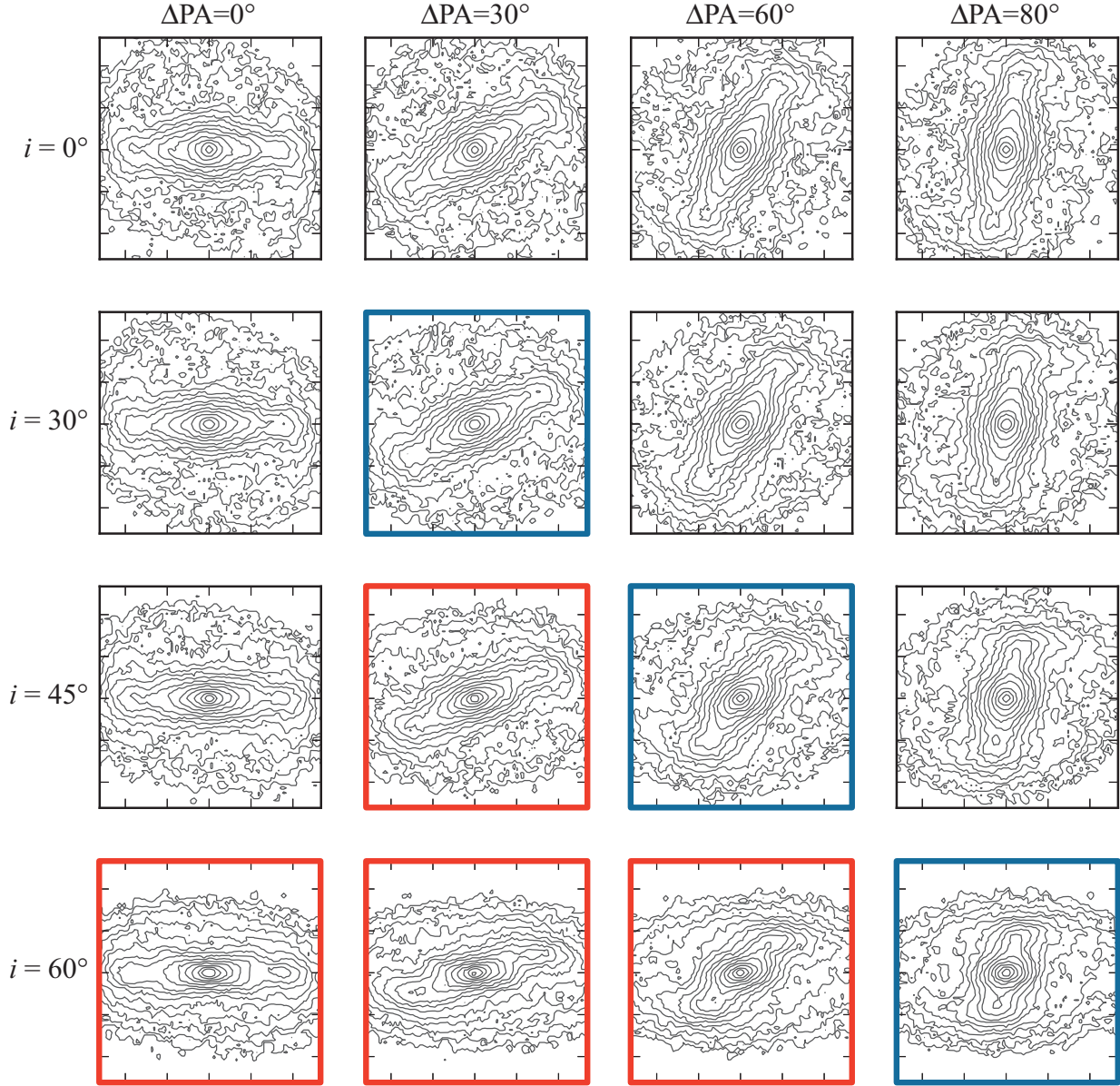


Figure 5. Grid showing various projections of *N*-body model A. From left to right, the projections show the bar rotated with respect to the line of nodes (ΔPA). The simulation is projected at increasing inclinations as one goes from the top row (face-on) to the bottom ($i = 60^\circ$); the disc line of nodes is horizontal in all panels. Thick red lines outline panels where some version of the box+spurs morphology is clearly visible; thick blue lines outline panels where weaker versions of this morphology are (possibly) visible.

box/peanut structures, even if they do not match exactly the strong, paradigmatic form presented in Section 2.1. For example, as ΔPA gets larger, we move from a situation where the spurs appear to be parallel to the boxy zone to one where the spurs appear to proceed from the *corners* of the boxy zone at some intermediate angle (e.g., the $i = 60^\circ$ row of Figure 5, where this alternate morphology is clearly present for $\Delta PA = 60^\circ$.) This is shown more directly in Figure 6, where we compare several real galaxies having inclinations $\sim 50\text{--}60^\circ$ with projections of the same *N*-body simulation.

Figure 6 also illustrates how the basic features of the box+spurs morphology in *real* galaxies can be reproduced by *N*-body models. Even though fine details may vary from galaxy to galaxy – e.g., the relative size of the boxy zone

compared with the length of the spurs, the apparent thickness of the spurs, etc. – the same *N*-body model does an impressive job of matching the basic isophote patterns in four different galaxies.

3.2 Matching Isophotal Features with 3D Stellar Structure in the Box/Peanut

It seems clear that we can identify the boxy zone in the box+spurs morphology with the projection of the vertically thick B/P structure, and the spurs with the projection of outer, vertically thin part of the bar. Can we quantify this? In particular: can we devise a measurement of the boxy zone

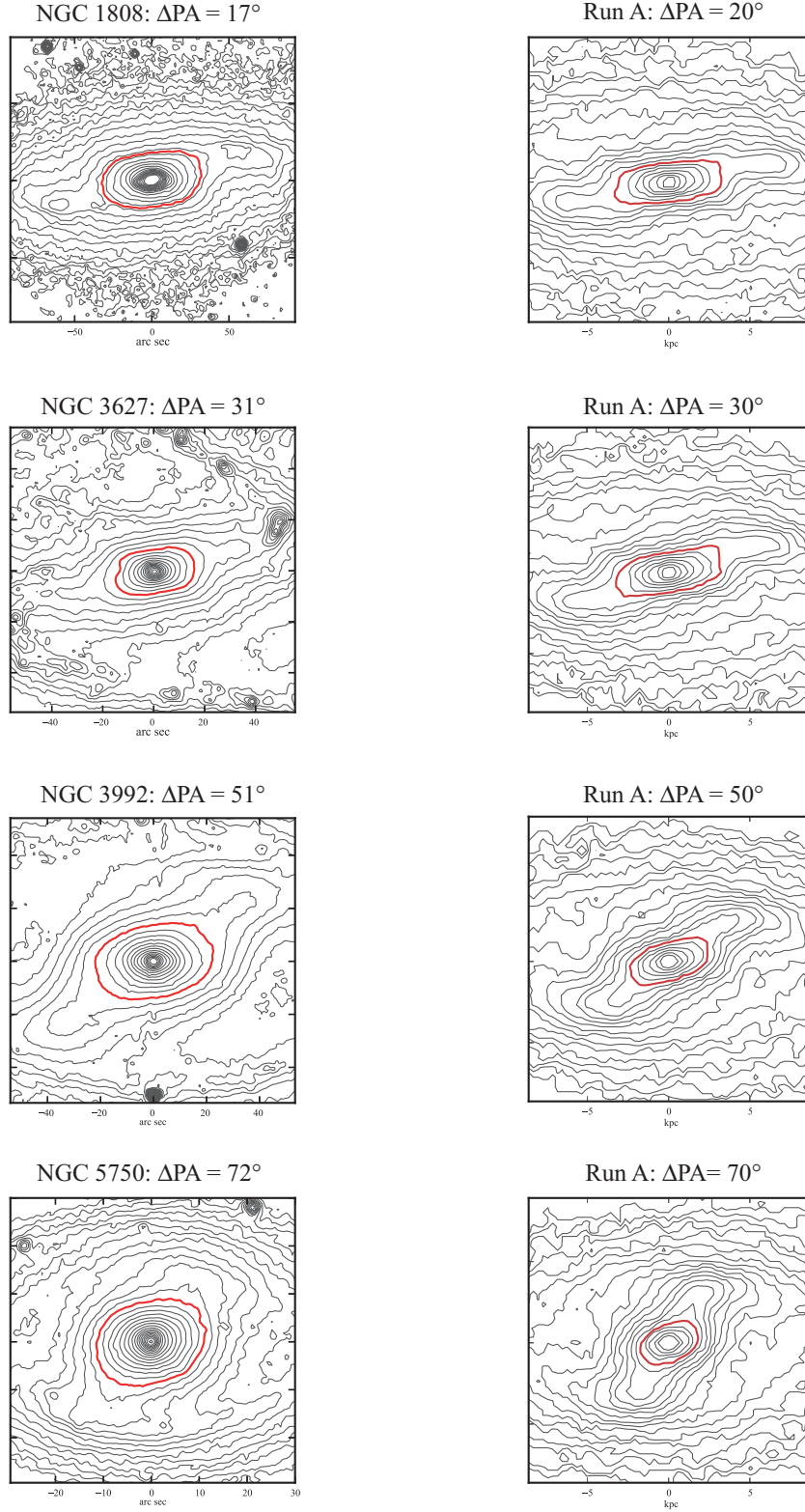


Figure 6. Comparison of real galaxies and N -body models, and a demonstration of how the offset spurs “rotate” from aligned with the major axis of the inner, boxy zone (outlined in red) to projecting at an angle as the bar rotates further away from the major axis. **Left panels:** Examples of real galaxies (all with inclinations between 50° and 65°) where the (deprojected) angle ΔPA between the bar and the disc line of nodes increases from top to bottom. All images have been rotated to make the disc major axis horizontal; the plots of NGC 3627 and NGC 3992 has also been reflected about the vertical axis. (Images are H -band for NGC 1808 and *Spitzer* IRAC1 for the others.) **Right panels:** Same, but now showing projections of N -body model A at $i = 60^\circ$.

which corresponds to a measurement of the 3D B/P structure?

After considerable experimentation, we settled on a direct visual measurement of the extent of the boxy region: R_{box} . This is the radius from the centre of the galaxy along the bar major axis (more specifically, along the major axis of the boxy-region isophotes) beyond which the spurs dominate. There is inevitably some ambiguity in measuring this radius, but we find that it can usually be determined with a precision of $\sim 10\%$, which is at least roughly comparable to the uncertainty in determining the overall length of the bar. Examples of R_{box} measurements on real galaxies are given in Figures 7, while examples using projected N -body models are given in Figure 8. Additional examples using the isophotes of real galaxies are presented in Figure 10 and in the Appendix.

Figure 8 shows measurements of R_{box} on two moderately inclined projections of run A (left-hand panels). The middle panels of that figure show something inaccessible for real galaxies with moderate inclinations: the edge-on view of the simulation, with the bar perpendicular to the line of sight, showing the full B/P structure. Parallel cuts through the edge-on view are shown in the bottom middle panel. We measured R_{box} on a number of different projections (varying inclination and bar ΔPA); the mean of the deprojected values for this simulation was 4.8 kpc. This radius is marked in the middle panels by the vertical dashed red lines. (The right-hand panels show the result of the same exercise for another simulation.) Although one could argue that the deprojected R_{box} measurement slightly underestimates the full radial extent of the B/P structure, it is none the less a surprisingly good match. The very upper part of the B/P structure may extend slightly beyond the boxy zone into the spurs, but the majority of the stars making up the bar at this radius are in planar orbits, so the bar is predominantly flat at this point.

In Figure 8 we also plot the radius where z_4 , the fourth-order Gauss-Hermite moment of the vertical density distribution along the bar major axis, reaches a minimum. This is a measurement of the B/P structure used by Debattista et al. (2005)⁴ and Méndez-Abreu et al. (2008), who found that it closely matched the minimum in h_4 , the fourth-order Gauss-Hermite moment of the stellar *velocity* distribution, something which could be measured in face-on bars using spectroscopy. We note that the radius of minimum z_4 is usually *smaller* than R_{box} , something which should be kept in mind when comparing spectroscopic measurements of face-on bars with our morphological measurements.

3.3 Can We Use Ellipse Fits to Identify and Measure Inclined Box/Peanut Structures?

Strong versions of the boxy-bar morphology (e.g., Figures 1 and 2) are rather easy to spot from visual inspection of the isophotes, and measuring the size of the boxy region on images of such galaxies is not too difficult. It would clearly be desirable, however, to have a consistent set of criteria which could be applied in a semi-automated fashion to images, so that one could more easily identify weaker exam-

ples. Since the process of fitting ellipses to galaxy isophotes is widespread and easily done, it would be convenient if we could use ellipse fits for this purpose, and even more so if we could define a way to measure R_{box} using ellipse fits. The fact that ellipse fits have traditionally been used to identify “boxy” isophotes in elliptical galaxies would seem to suggest that they could be useful here as well.

Unfortunately, considerable experimentation with ellipse fits to isophotes of both projected N -body models and real galaxies has forced us to conclude that ellipse-fitting does not provide a simple solution. While we *can* devise a set of criteria which will often – but not always – indicate the *presence* of a boxy bar (and thus the projected B/P structure), attempts to devise a simple measurement of the boxy zone’s size run into problems.⁵

We digress briefly to remind the reader of how ellipse fits are constructed and analysed. The process of ellipse fitting involves finding an ellipse of a given semi-major axis a which best fits a given galaxy isophote, given the ability to vary the ellipse’s centre, position angle, and semi-minor axis b . The particular implementation we use is that of the IRAF task ELLIPSE, part of the STSDAS package and based on the approach of Jedrzejewski (1987). If an ellipse is a perfect fit to the isophote, then the intensity along the ellipse will be constant. In practice, this is never true, so the variations in intensity along the ellipse can be expanded as a Fourier sum:

$$I(\theta) = I_0 + \sum_{n=1}^{\infty} [\tilde{A}_n \sin n\theta + \tilde{B}_n \cos n\theta], \quad (1)$$

where θ is the eccentric anomaly. For a best-fitting ellipse, the first- and second-order coefficients will be zero. In order to describe how the isophote differs *spatially* from the fitted ellipse, the higher-order ($n \geq 3$) coefficients are divided by the local radial intensity gradient and by the ellipse semi-major axis. This transforms them into normalized coefficients of *radial* deviation δr from a perfect ellipse, in a coordinate system where the fitted ellipse is a circle with radius $r = (ab)^{1/2}$:

$$\frac{\delta r(\theta)}{r} = \sum_{k=3}^4 [A_k \sin k\theta + B_k \cos k\theta]. \quad (2)$$

The most commonly used higher-order coefficient is B_4 , the $\cos 4\theta$ term, which measures symmetric distortions from pure ellipticity along the ellipse major axis. When $B_4 > 0$, the isophotes are pointed or “discy”; when $B_4 < 0$, the isophotes have a more rectangular or “boxy” shape. Note that some other ellipse-fitting codes (e.g., that of Bender, Döbereiner, & Möllenhoff 1988), designate the $\sin 4\theta$ and $\cos 4\theta$ terms by b_4/a and a_4/a , respectively.⁶

One might expect that the boxy zone would be marked in the ellipse fits by negative B_4 values, transitioning to more elliptical – even discy – isophotes outside. This is often true, and Figure 9 shows some examples of the pattern. In

⁵ This discussion is based on ellipse fits of galaxies listed in Table 1, galaxies found in the analysis of our “local sample” in Section 4, and N -body models.

⁶ The conversion between the different $\cos 4\theta$ coefficients is $a_4/a = \sqrt{b/a} B_4$ (Bender et al. 1988).

⁴ Referred to as d_4 in that paper.

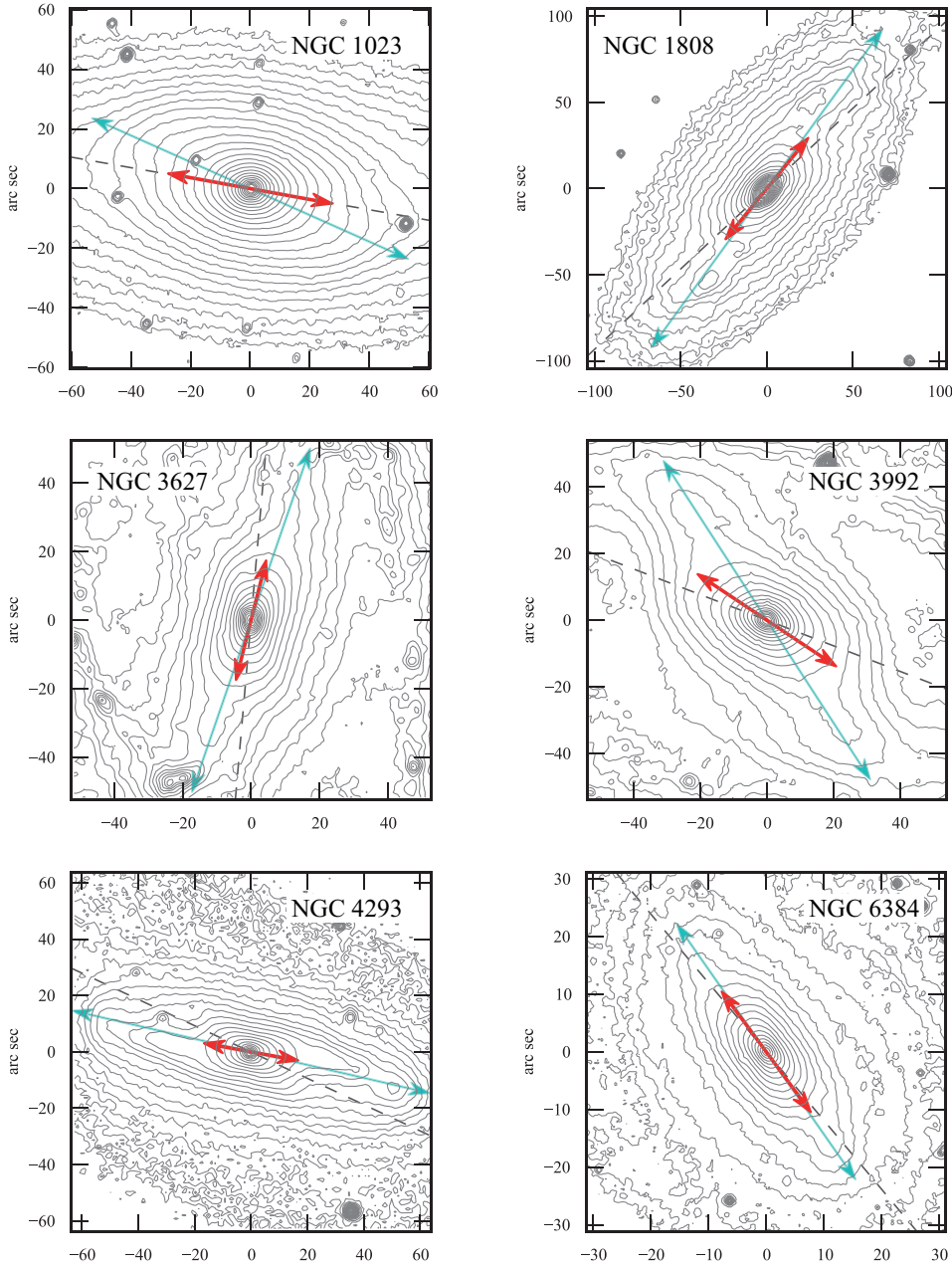


Figure 7. Examples of R_{box} measurements for six galaxies. In each panel, the red arrows indicate the position angle and size of the boxy region, $2 \times R_{\text{box}}$; the longer cyan arrows indicate the position angle and full size of the bar. Thin black dashed lines indicate position angle of line of nodes. North is up and East is to the left in all panels. See also Figures 8 and 10, and the Appendix. (See Appendix for image sources.)

some galaxies, however, the isophotes may never become boxy enough to acquire negative B_4 values.

The A_4 term (the $\sin 4\theta$ coefficient) is also useful, because it can indicate the presence of offset spurs. Nonzero A_4 values mean that the fitted isophote has deviations from bisymmetry (e.g., transforming the symmetric rectangular shape into something more like a parallelogram): when $A_4 > 0$, the isophote ends are offset counter-clockwise from the major axis of the fitted ellipse, and when $A_4 < 0$, they are offset clockwise; see Figure 10.

Thus, a reasonable set of criteria for identifying the boxy-bar morphology might include the following:

- (i) The presence of an inner boxy region: $B_4 < 0$ somewhere inside the bar. (In some cases, the “boxy” region will be close to elliptical, with $B_4 \approx 0$.)
- (ii) This region corresponds to a value of A_4 near zero and (sometimes) to a plateau or shoulder in the position-angle profile. This is the region of symmetric, boxy isophotes, corresponding to the projected box/peanut.
- (iii) At larger radii (but still inside the bar), the isophotes become *discy* ($B_4 > 0$); this is the region of the spurs outside

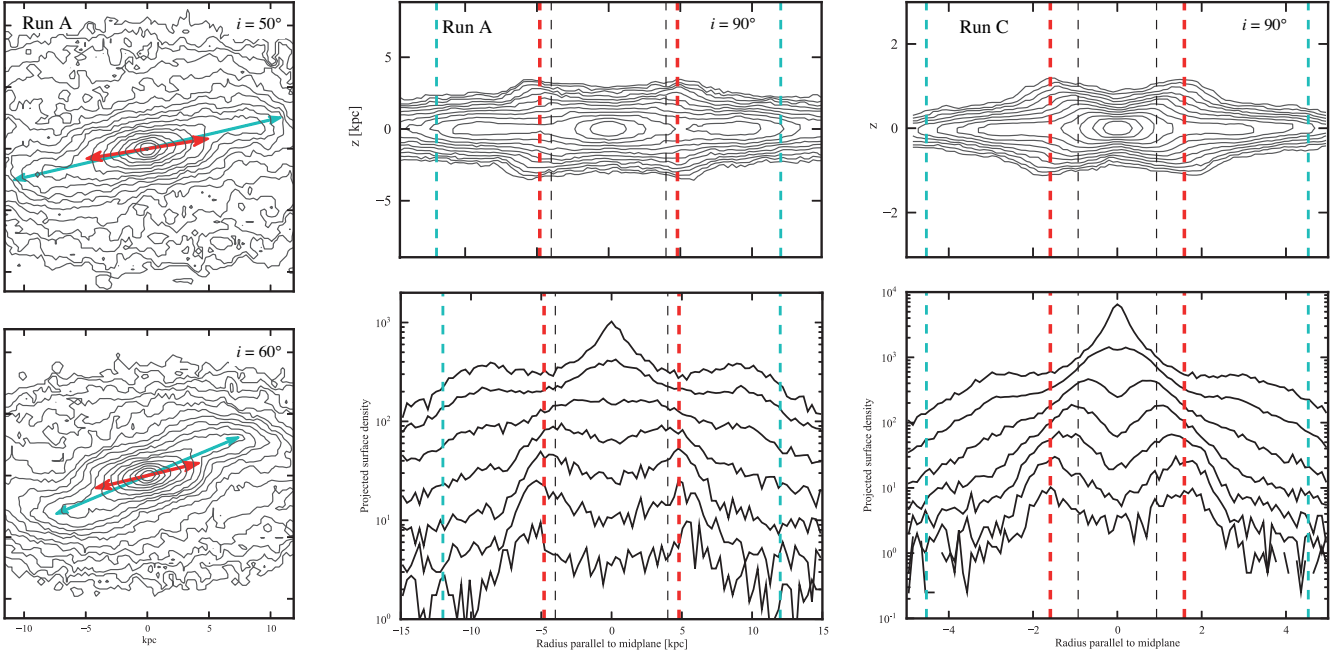


Figure 8. Matching 2D morphology in moderate-inclination projections with 3D morphology. **Left panels:** Projections of N -body model A, at $i = 50^\circ$, bar $\Delta\text{PA} = 20^\circ$ (top) and $i = 60^\circ$, bar $\Delta\text{PA} = 40^\circ$ (bottom). Red arrows mark the measured R_{box} values; longer cyan arrows mark the full bar radius. **Middle panel – top:** Edge-on view of the same simulation, with the bar oriented perpendicular to the line of sight. **Middle panel – bottom:** Cuts through the edge-on view, parallel to the galaxy midplane (from top to bottom, the profiles are at $|z| = 0, 0.9, 1.5, 2.1, 2.7, 3.3$, and 3.9 kpc). In both panels, thin vertical black lines mark the $\min(z_4)$ radius, vertical red lines mark the average (deprojected) value of R_{box} from measurements on moderately inclined projections (e.g., left panels), and vertical cyan lines mark full bar radius. **Right panels:** Same as middle panels, but showing model C at $t = 600$ (parallel cuts at $|z| = 0, 0.3, 0.5, 0.7, 0.9, 1.1$, and 1.3). Taken together, these show that R_{box} , measured on moderately inclined images, is a reasonable estimate of the extent of the B/P structure, as seen in the edge-on views.

the boxy zone, corresponding to the flat part of the bar outside the box/peanut.

(iv) Almost always, the A_4 term becomes significantly nonzero in the same region, and the position angle continues to change; in at least some cases, the extremum in A_4 happens slightly *inside* the peak in B_4 . This is the signature of *offset* spurs, which indicates that the bar is not aligned with the galaxy line of nodes. (Spurs which are aligned would be indicated by $A_4 = 0$; this means that the bar lies along the line of nodes.)

The preceding set of criteria suggest an appealingly simple correspondence: boxy zone = boxy isophotes (i.e., $B_4 < 0$), spurs = discy isophotes (i.e., $B_4 > 0$). So could we simply use the semi-major axis of maximum boxyness (minimum B_4) to derive R_{box} ? Or, alternately, could we use the semi-major axis where B_4 crosses from negative to positive?

In practice, this simple idea does not work for most galaxies. Figure 10 shows that the $\min(B_4)$ measurement usually *underestimates* R_{box} (the size of the boxy zone). And the $B_4 = 0$ semi-major axis turns out to correspond to an isophote which is actually well into the spur-dominated region, thus strongly *overestimating* R_{box} . In other words, even outside the boxy region, where the spurs are clearly present, the best-fitting ellipses can be sufficiently affected by the boxy region so as to have boxy deviations.⁷

⁷ We also observe that it is in general not wise to assume that

As a compromise, we have found that the *mean* of $a(\min(B_4))$ and $a(B_4 = 0)$ is often a reasonable approximation of R_{box} . So if one *must* use an ellipse-fit-based method for estimating R_{box} , one could certainly do worse than to use this. It *does* start to fail systematically when the bar is close to the galaxy minor axis, however (overestimating R_{box} ; see NGC 4340 in Figure 10), so we recommend measuring R_{box} directly on the image or isophotes whenever possible.

4 EXPLORING A LOCAL SAMPLE

While the list of boxy-bar galaxies in Table 1 is of potential use in providing candidates for detailed individual investigations, its heterogeneous nature tells us little about how common such features actually are. In this section, we focus on a well-defined local sample of barred galaxies and attempt to determine the frequency of the boxy-bar phenomenon.

The sample we use consists of nearby S0–Sb galaxies with bars, taken from the combined S0–Sb sample presented in Erwin et al. (2008) and Gutiérrez et al. (2011). This sample was defined so as to include all galaxies from the UGC catalog (Nilson 1973) which met the following criteria: RC3 major-axis diameter $D_{25} \geq 2.0'$, RC3 axis ratio $a/b \leq 2.0$, redshift $V \leq 2000 \text{ km s}^{-1}$ (from NED), and

isophotes with $B_4 = 0$ are always actually *elliptical*; they can be strongly non-elliptical.

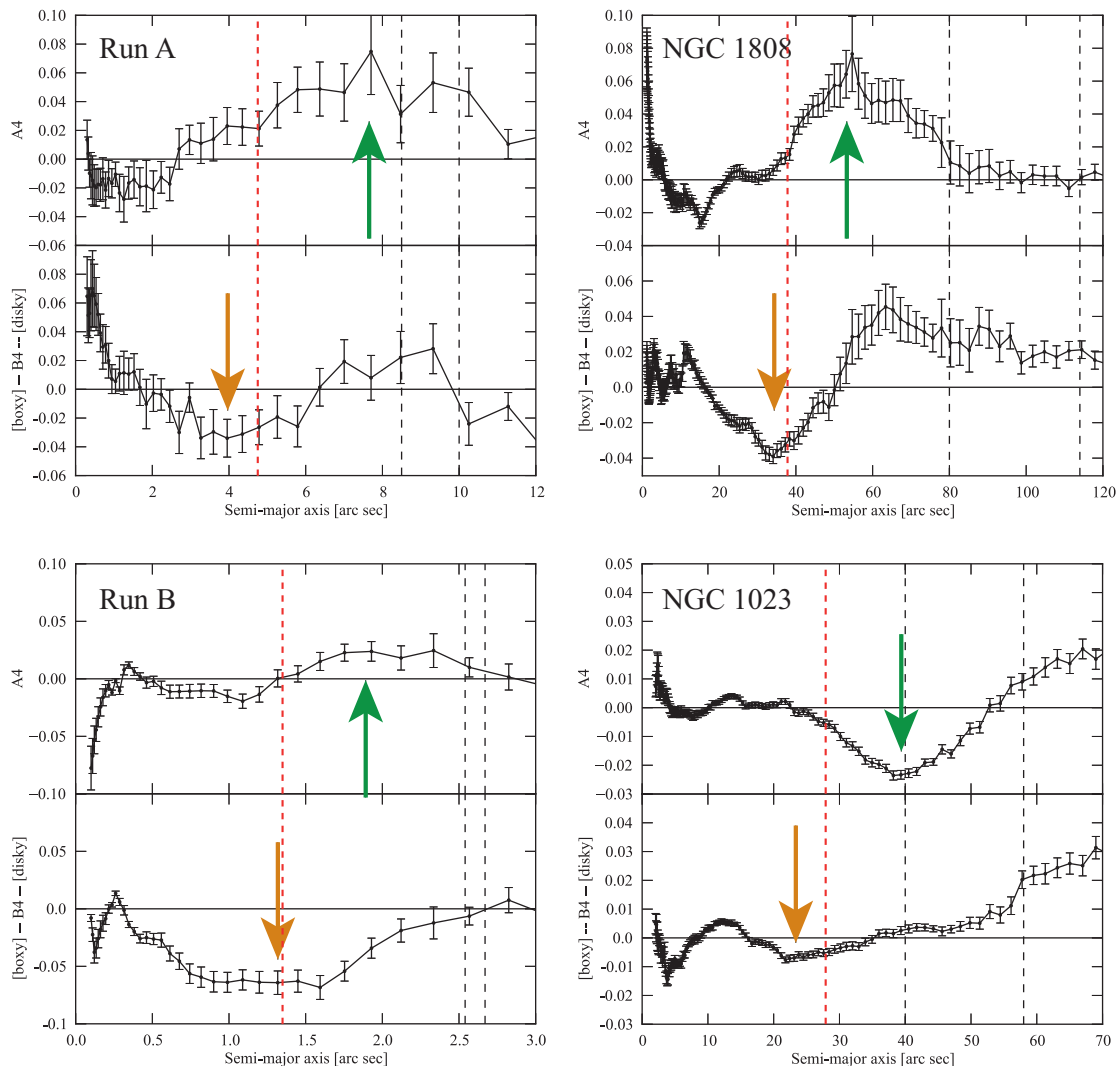


Figure 9. Signatures of box+spurs morphology in ellipse fits, using A_4 ($\sin 4\theta$) and B_4 ($\cos 4\theta$) coefficients. Vertical dashed black lines mark semi-major axes of our two estimates of bar size (a_e and L_{bar}); vertical short-dashed red lines mark R_{box} , our visual measurement of the size of the boxy region. **Left panels:** Ellipse fits to N -body simulations. Upper panel: run A, seen with $i = 60^\circ$, $\Delta\text{PA} = 20^\circ$; lower panel: run B at $t = 1000$, seen with $i = 45^\circ$, $\Delta\text{PA} = 40^\circ$. **Right panels:** Ellipse fits to real galaxies. Upper panel: NGC 1808, a strong boxy-bar case (see Figure 6); lower panel: NGC 1023, a much weaker case. In all panels, there a pattern of boxy isophotes ($B_4 < 0$) at small radii (gold arrows), transitioning at larger radii to discy isophotes ($B_4 > 0$) as the spurs become more prominent; at the same time, A_4 becomes strongly nonzero closer to the bar end (green arrows), indicating the offset orientation of the spurs.

declination $\geq -10^\circ$; S0 galaxies in the Virgo Cluster were also included (based on membership in the Virgo Cluster Catalog; Binggeli et al. 1985), ignoring the redshift limit. This produced a total of 122 galaxies, of which nine were excluded for being highly disturbed (e.g., merger remnants or polar-ring systems) or edge-on despite their low axis ratios (e.g., S0 galaxies with large bulges); see Erwin (2005) and Gutiérrez et al. (2011) for specifics. Of the remaining 113 galaxies, 78 proved to have bars; measurements of the bar parameters (size, position angle, maximum isophotal ellipticity) are presented in Erwin (2005), Erwin et al. (2008), and Gutiérrez et al. (2011), along with disc measurements.⁸

An axis ratio limit of $a/b \leq 2.0$ is the same as that

commonly used to maximize the identification (and measurement) of bars, and formally corresponds to inclinations $\lesssim 62^\circ$, assuming an intrinsic axis ratio of $c/a = 0.2$. Detailed analyses of individual galaxies showed that some probably have inclinations as high as 66° , but we did not attempt to exclude these systems.

One of the main virtues of such a locally defined sample is the high spatial resolution it affords. Even when we are restricted to images with seeing FWHM $\sim 1.5\text{--}2''$, this is significantly smaller than the typical sizes of bars in our sample (see Erwin 2005; Gutiérrez et al. 2011); in addition, *HST* images are available for many of the galaxies, which helps with resolving the structure of the smaller bars.

⁸ For NGC 2712, we use an updated disc position angle of 178° .

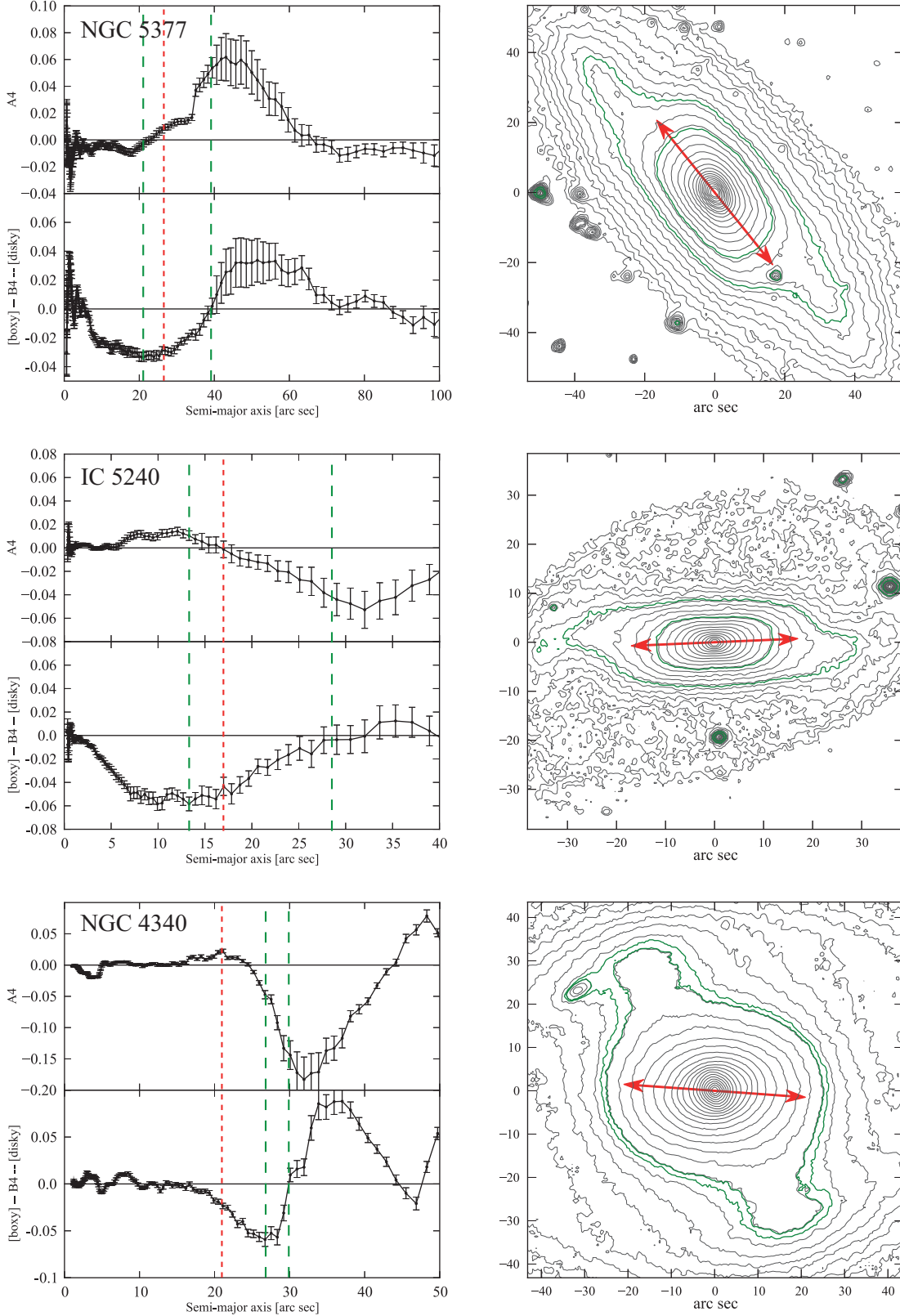


Figure 10. Why ellipse fits are problematic for measuring B/P sizes. **Left:** A_4 ($\sin 4\theta$) and B_4 ($\cos 4\theta$) coefficients from ellipse fits. Vertical green long-dashed lines mark semi-major axes corresponding to the maximally boxy ($\min(B_4)$) isophote and the isophote where $B_4 = 0$ immediately outside. Vertical short-dashed red lines indicate R_{box} , our visual measurement of the size of the boxy region. **Right:** Log-scaled isophotes of NGC 5377 (IRAC1, outer disc excluded), IC 5240 (K -band), and NGC 4340 (SDSS r -band); N is up and E is to the left. Red arrows mark the boxy region ($2 \times R_{\text{box}}$); thicker green lines outline isophotes corresponding to the $\min(B_4)$ and $B_4 = 0$ fitted ellipses. Neither $\min(B_4)$ nor $B_4 = 0$ can be used to reliably and accurately define the limits of the boxy region.

Table 2. Local Barred-Galaxy Sample

| Name (1) | Type (2) | Distance (3) | M_B (4) | i (5) | ΔPA (6) | Boxy (7) | Spurs (8) | Offset (9) | Lead/Trail (10) |
|-------------|--------------------------|-----------------|--------------|------------|--------------------|-------------|--------------|---------------|--------------------|
| NGC 278 | SAB(rs)b | 11.0 | -19.40 | 17 | 51 | no | no | — | — |
| NGC 718 | SAB(s)a | 22.6 | -19.43 | 30 | 37 | no | no | — | — |
| NGC 936 | SB(rs)0 ⁺ | 23.0 | -20.86 | 41 | 57 | no | no | — | — |
| NGC 1022 | (R')SB(s)a | 18.1 | -19.46 | 24 | 61 | yes | yes | yes | trail |
| NGC 1068 | (R)SA(rs)b | 14.2 | -21.23 | 31 | 76 | no | no | — | — |
| NGC 2273 | SB(r)a: | 27.3 | -20.11 | 50 | 74 | no | no | — | — |
| NGC 2681 | (R')SAB(rs)0/a | 17.2 | -20.20 | 18 | 71 | no | no | — | — |
| NGC 2712 | SB(r)b: | 26.5 | -19.88 | 59 | 53 | yes | yes? | yes | trail |
| NGC 2787 | SB(r)0 ⁺ | 7.5 | -18.20 | 55 | 65 | no | no | — | — |
| NGC 2859 | (R)SB(r)0 ⁺ | 24.2 | -20.21 | 32 | 79 | no | no | — | — |
| NGC 2880 | SB0 ⁻ | 21.9 | -19.38 | 52 | 72 | no | no | — | — |
| NGC 2950 | (R)SB(r)0 ⁰ | 14.9 | -19.14 | 48 | 48 | no? | no? | — | — |
| NGC 2962 | (R)SAB(rs)0 ⁺ | 30.0 | -19.71 | 53 | 30 | yes? | yes? | yes | — |
| NGC 3031 | SA(s)ab | 3.6 | -20.73 | 58 | 18 | yes | yes? | yes | lead |
| NGC 3049 | SB(rs)ab | 20.2 | -18.65 | 51 | 8 | no | no | — | — |
| NGC 3185 | (R)SB(r)a | 17.5 | -18.61 | 49 | 37 | yes | yes | yes | lead |
| NGC 3351 | SB(r)b | 10.0 | -19.94 | 46 | 82 | no | no | — | — |
| NGC 3368 | SAB(rs)ab | 10.5 | -20.37 | 50 | 67 | yes | yes? | yes? | lead? |
| NGC 3412 | SB(s)0 ⁰ | 11.3 | -18.98 | 58 | 68 | no | no | — | — |
| NGC 3485 | SB(r)b: | 20.0 | -19.03 | 26 | 43 | no | no? | — | — |
| NGC 3489 | SAB(rs)0 ⁺ | 12.1 | -19.45 | 58 | 72 | no | no | — | — |
| NGC 3504 | (R)SAB(s)ab | 22.3 | -20.29 | 22 | 6 | no | no | — | — |
| NGC 3507 | SB(s)b | 14.2 | -19.21 | 27 | 24 | no | no | — | — |
| NGC 3599 | SA0 ⁰ | 19.8 | -18.70 | 22 | 62 | no | no | — | — |
| NGC 3626 | (R)SA(rs)0 ⁺ | 19.5 | -19.75 | 49 | 11 | yes? | yes | yes | lead |
| NGC 3729 | SB(r)a pec | 16.8 | -19.35 | 53 | 50 | yes | yes | yes | lead |
| NGC 3941 | SB(s)0 ⁰ | 12.2 | -19.31 | 52 | 33 | yes? | yes? | yes | — |
| NGC 3945 | (R)SB(rs)0 ⁺ | 19.8 | -19.94 | 55 | 88 | no | no | — | — |
| NGC 3982 | SAB(r)b: | 20.9 | -19.95 | 29 | 8 | no | no | — | — |
| NGC 3998 | SA(r)0 ⁰ | 13.7 | -19.36 | 38 | 13 | no | no | — | — |
| NGC 4037 | SB(rs)b: | 13.5 | -17.79 | 32 | 46 | yes | yes? | yes? | trail |
| NGC 4045 | SAB(r)a | 26.8 | -19.70 | 48 | 78 | no? | no? | — | — |
| NGC 4102 | SAB(s)b? | 14.4 | -19.22 | 55 | 44 | yes? | yes? | yes | trail |
| NGC 4143 | SAB(s)0 ⁰ | 15.9 | -19.40 | 59 | 34 | yes? | no? | — | — |
| NGC 4151 | (R')SAB(rs)ab: | 15.9 | -20.70 | 20 | 73 | no | no | — | — |
| NGC 4203 | SAB0 ⁻ | 15.1 | -19.21 | 28 | 2 | no | no | — | — |
| NGC 4245 | SB(r)0/a | 12.0 | -18.28 | 38 | 43 | no | no? | — | — |
| NGC 4267 | SB(s)0 ⁻ ? | 15.3 | -19.25 | 25 | 86 | no | no | — | — |
| NGC 4314 | SB(rs)a | 12.0 | -19.12 | 25 | 82 | no | no | — | — |
| NGC 4319 | SB(r)ab | 23.5 | -19.26 | 42 | 22 | yes | yes? | yes? | lead |
| NGC 4340 | SB(r)0 ⁺ | 15.3 | -18.90 | 50 | 73 | yes | yes | yes | — |
| NGC 4369 | (R)SA(rs)a | 16.6 | -18.84 | 18 | 78 | no | no | — | — |
| NGC 4371 | SB(r)0 ⁺ | 15.3 | -19.32 | 58 | 85 | no | no | — | — |
| NGC 4386 | SAB0 ⁰ : | 27.0 | -19.68 | 48 | 9 | yes? | yes? | yes | — |
| NGC 4477 | SB(s)0 ⁰ ?: | 15.3 | -19.69 | 33 | 71 | no | no? | — | — |
| NGC 4531 | SB0 ⁺ : | 15.2 | -18.67 | 49 | 38 | no | no | — | — |
| NGC 4596 | SB(r)0 ⁺ | 15.3 | -19.63 | 42 | 55 | no | no | — | — |
| NGC 4608 | SB(r)0 ⁰ | 15.3 | -19.02 | 36 | 78 | no | no | — | — |
| NGC 4612 | (R)SAB0 ⁰ | 15.3 | -19.01 | 44 | 67 | no | no | — | — |
| NGC 4643 | SB(rs)0/a | 18.3 | -19.85 | 38 | 82 | no | no | — | — |
| NGC 4665 | SB(s)0/a | 10.9 | -18.87 | 26 | 66 | no | no | — | — |
| NGC 4691 | (R)SB(s)0/a pec | 15.1 | -19.43 | 38 | 58 | no | no | — | — |
| NGC 4699 | SAB(rs)b | 18.9 | -21.37 | 42 | 17 | yes? | yes | yes? | trail? |
| NGC 4725 | SAB(r)ab pec | 12.4 | -20.69 | 42 | 13 | yes | yes | yes | trail |

Notes on the presence or absence of boxy-bar features in a local sample of S0–Sb barred galaxies.

(1) Galaxy name. (2) Hubble type from RC3. (3) Distance in Mpc (for sources, see Erwin et al. 2008; Gutiérrez et al. 2011). (4) Absolute B magnitude, from HyperLeda B_{tc} and our adopted distance. (5) Galaxy inclination. (6) Deprojected angle between bar and disc major axis. (7) Indicates whether bar displays boxy interior. (8) Indicates whether narrow spurs outside boxy interior are seen. (9) Indicates whether spurs, if present, are offset from major axis of boxy interior. (10) Indicates whether offset spurs, if present, lead or trail (assuming main spiral pattern is trailing).

Table 2. Continued

| Name (1) | Type (2) | Distance (3) | M_B (4) | i (5) | ΔPA (6) | Boxy (7) | Spurs (8) | Offset (9) | Lead/Trail (10) |
|-------------|------------------------|-----------------|--------------|------------|--------------------|-------------|--------------|---------------|--------------------|
| NGC 4736 | (R)SA(r)ab | 5.1 | -19.98 | 35 | 27 | no | no | — | — |
| NGC 4750 | (R)SA(rs)ab | 25.4 | -20.27 | 30 | 43 | no | no | — | — |
| NGC 4754 | SB(r)0 ⁻ : | 16.8 | -19.78 | 62 | 75 | no | no | — | — |
| NGC 4772 | SA(s)a | 14.5 | -19.22 | 44 | 16 | no? | no? | — | — |
| NGC 4941 | (R)SAB(r)ab: | 15.0 | -19.37 | 48 | 6 | no? | no? | — | — |
| NGC 4995 | SAB(r)b | 23.6 | -20.41 | 47 | 74 | yes? | yes | yes | trail |
| NGC 5338 | SB0 ⁰ : | 12.8 | -16.70 | 66 | 55 | no? | no? | — | — |
| NGC 5377 | (R)SB(s)a | 27.1 | -20.29 | 59 | 35 | yes | yes | yes | trail |
| NGC 5701 | (R)SB(rs)0/a | 21.3 | -19.97 | 20 | 50 | no | no | — | — |
| NGC 5740 | SAB(rs)b | 22.0 | -19.67 | 60 | 57 | yes | yes | yes | trail |
| NGC 5750 | SB(r)0/a | 26.6 | -19.94 | 62 | 72 | yes | yes? | yes? | trail |
| NGC 5806 | SAB(s)b | 19.2 | -19.67 | 58 | 13 | yes | yes | yes | trail |
| NGC 5832 | SB(rs)b? | 9.9 | -17.15 | 55 | 76 | no? | no? | — | — |
| NGC 5957 | (R')SAB(r)b | 26.2 | -19.36 | 15 | 3 | no? | no? | — | — |
| NGC 6012 | (R)SB(r)ab: | 26.7 | -19.78 | 33 | 59 | no | no | — | — |
| NGC 6654 | (R')SB(s)0/a | 28.3 | -19.65 | 44 | 23 | no | no? | — | — |
| NGC 7177 | SAB(r)b | 16.8 | -19.79 | 48 | 76 | no? | no? | — | — |
| NGC 7280 | SAB(r)0 ⁺ | 24.3 | -19.16 | 50 | 28 | no | no | — | — |
| NGC 7743 | (R)SB(s)0 ⁺ | 20.7 | -19.49 | 28 | 11 | yes? | yes? | yes | lead |
| IC 499 | Sa | 29.5 | -19.37 | 59 | 47 | no? | no | — | — |
| IC 676 | (R)SB(r)0 ⁺ | 19.4 | -18.42 | 47 | 41 | no? | yes? | yes? | lead |
| IC 1067 | SB(s)b | 22.2 | -18.82 | 44 | 40 | yes | yes | yes | trail |
| UGC 3685 | SB(rs)b | 26.8 | -19.51 | 31 | 14 | no | no | — | — |
| UGC 11920 | SB0/a | 18.0 | -19.71 | 52 | 8 | no? | no? | — | — |

4.1 Analysis

We analysed the best available images for all galaxies in the sample to determine if they showed evidence for the boxy-bar morphology; we counted both the strong examples discussed in Section 2 and weaker examples suggested by some of the N -body projections (e.g., cases where the spurs are short and/or project from corners of the boxy zone). Our primary method of analysis was visual inspection of the images, and of isophote contour plots derived from the images. (The suggested ellipse-fit-based method we discuss in Section 3.3 was derived *after* this analysis, using galaxies identified visually, including those found in this sample.)

For dust-free S0 galaxies, we generally used red (R , r , or i) optical images from the SDSS (DR7) or from other sources discussed in Erwin & Sparke (2003), Erwin et al. (2008), and Gutiérrez et al. (2011). For galaxies with dust obscuration in the bar region – including almost all of the spiral galaxies – we used near-IR imaging from a variety of sources, the most common being *Spitzer* IRAC1 (3.6 μ m) images from NED or from the *Spitzer* archive. Most of the *Spitzer* images are part of the *Spitzer* Survey of Stellar Structure in Galaxies (Sheth et al. 2010, S⁴G); other sources included SINGS (Kennicutt et al. 2003), and the *Spitzer* Local Volume Legacy (Dale et al. 2009). We also used H and K images available from NED (mostly higher in resolution or S/N than IRAC1 images), including those from Knapen et al. (2003), Eskridge et al. (2002), Möllenhoff & Heidt (2001), and Wu et al. (2002), and a set of J and H images taken with the INGRID imager on the William Herschel Telescope (e.g., Erwin et al. 2003; Nowak et al. 2010). Finally, for some galaxies with particularly small bars (e.g., NGC 4102) we used archival *HST* NICMOS2 and NICMOS3 images, mostly obtained with the F160W filter. The median resolution of the images we used

was FWHM = 1.1'', with a range of 0.5–2.0'' (excluding the five galaxies for which we used *HST* NICMOS2 or NICMOS3 images).

The primary results of our analysis are coded in Table 2, where we indicate whether or not the bar of each galaxy⁹ has a boxy interior, and if so, whether it has spurs and whether the spurs are offset relative to the boxy zone. Less certain classifications are indicated by question marks. The offset of the spurs is defined as leading or trailing based on the sense of spiral arm rotation; this is not possible for some galaxies, such as S0 galaxies where the absence of dust lanes and spiral arms prevents us from determining a sense of rotation for the galaxy.

The left panel of Figure 11 shows how the fraction of galaxies with boxy-bar morphology depends on galaxy inclination. As we would expect, the fraction rises as we go to higher inclinations; for $i > 40^\circ$, roughly half of the bars have boxy interiors. What is perhaps unexpected is how *low* in inclination one can go and still detect boxy interiors: there are two galaxies with inclinations $20^\circ < i < 30^\circ$ where we find evidence for the boxy-bar structure: NGC 1022 ($i = 24^\circ$) and NGC 7743 ($i = 28^\circ$).

The right panel of the same figure shows the fraction of galaxies which have boxy-bar morphologies as a function of ΔPA , using the deprojected position angles. The boxy-bar morphology is clearly most common when the relative position angle is between 10° and 40° , and is rare for $\Delta PA > 60^\circ$. If we divide the sample into galaxies with $\Delta PA < 45^\circ$ (35 total) and galaxies with $\Delta PA > 45^\circ$ (43 total), the boxy-bar fractions are $43 \pm 8\%$ and $21^{+7}_{-6}\%$, respectively, though the

⁹ In the case of double-barred galaxies, we analyse the outer bar.

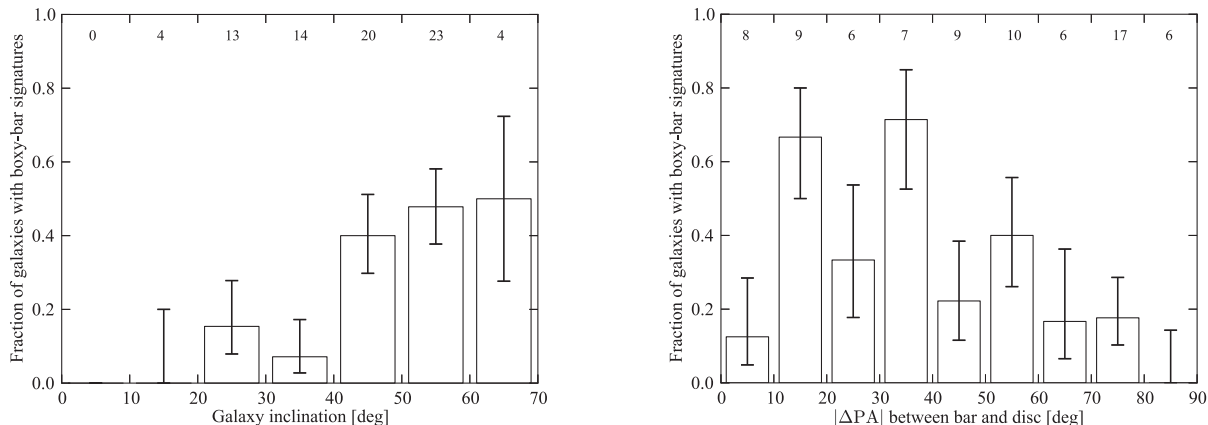


Figure 11. Left panel: Fraction of galaxies in our local sample (Table 2) with detected boxy-bar morphologies, as a function of galaxy inclination; the total number of galaxies in each inclination bin is listed along the top of the figure. **Right panel:** Same, but now showing fraction as a function of ΔPA , the (deprojected) relative angle between the bar and the galaxy major axis. Error bars in both panels are binomial uncertainties calculated using the method of Wilson (1927).

statistical significance of this difference is marginal (Fisher Exact Test $P = 0.049$).

4.2 What Fraction of Candidate Galaxies Have B/P Bulges?

Our analysis of the N -body simulations suggests that detection of the B/P structure is maximized both when the inclination is high and when the bar is closer to the major axis than to the minor axis. So if we are interested in finding out how common B/P structures are in our local sample, it makes sense to restrict ourselves to a subset of galaxies with reasonably high inclinations and low values of ΔPA .

For galaxies with $i \geq 40^\circ$ and $\Delta\text{PA} < 45^\circ$, we find that $64^{+10}_{-11}\%$ show at least a boxy interior; $59 \pm 10\%$ of the subsample show both a boxy interior and distinct spurs. (If we increase the inclination limit to 50° , the frequencies become $70^{+12}_{-16}\%$ and $60^{+14}_{-16}\%$, respectively.) This suggests that, roughly speaking, at least two-thirds of S0–Sb bars have buckled or otherwise thickened and produced B/P structures. The fraction may well be higher if some of the bars have relatively weak B/P structures, which do not produce a strong projected signature when the inclination is lower; significant bulges or central discs can potentially also weaken the apparent signature. We consider the possibility of identifying individual galaxies which might lack B/P structures altogether in Section 6.1.

5 THE SIZES OF BOX/PEANUT STRUCTURES RELATIVE TO BARS

For the 24 galaxies in our local sample where we found boxy-bar signatures, we measured the size of the boxy region R_{box} , as described in Section 3.2. In absolute terms, R_{box} ranges from 0.37 to 3.79 kpc, with a mean of 1.46 ± 0.91 kpc; these sizes are deprojected using the ellipse-fit position angle corresponding to the boxy region.

However, what is probably more interesting is the question of how much of any given bar is vertically thickened. To investigate this, we calculated the size of the boxy region relative to the length of the bar. All the local-sample galaxies have bar measurements in Erwin (2005) or Gutiérrez et al. (2011): a_e and L_{bar} (see Erwin 2005, for definitions and comparisons with N -body measurements). Of the two bar-length measurements, L_{bar} is probably more relevant, since it attempts to measure the full length of the bar; a_e (the semi-major axis of maximum ellipticity) is a lower limit which in most cases underestimates the true bar length. To compare R_{box} with L_{bar} , we deprojected both measurements; the deprojection of R_{box} was as described in the previous paragraph, while the deprojection of L_{bar} used the bar position angle from Erwin (2005) or Gutiérrez et al. (2011).

Figure 12 shows the distribution of $R_{\text{box}}/L_{\text{bar}}$ for our local sample. For the complete sample, we find a mean size of $R_{\text{box}}/L_{\text{bar}} = 0.38 \pm 0.08$ (median = 0.37); for the restricted subset of 15 galaxies with $\Delta\text{PA} < 45^\circ$, $\langle R_{\text{box}}/L_{\text{bar}} \rangle = 0.42 \pm 0.07$ (median = 0.43). Thus, it appears that on average box/peanut structures extend to slightly less than half the bar length. Values of $R_{\text{box}}/L_{\text{bar}}$ range from a low of 0.26 (0.29 for the $\Delta\text{PA} < 45^\circ$ subset) to a maximum of 0.58. Given the relatively narrow distribution in Figure 12, it is not surprising that R_{box} and L_{bar} are strongly correlated (Spearman $r = 0.92$, $P = 1.3 \times 10^{-10}$ for the complete local sample¹⁰). If we include an additional twelve galaxies not in our sample where we have measured both R_{box} and L_{bar} , the statistics do not change significantly: $\langle R_{\text{box}}/L_{\text{bar}} \rangle = 0.38 \pm 0.07$ (median = 0.38). If, instead, we use a_e for the bar size, the mean values are $R_{\text{box}}/a_e = 0.53 \pm 0.09$ for the local sample with $\Delta\text{PA} < 45^\circ$ and $R_{\text{box}}/a_e = 0.47 \pm 0.11$ for all values of ΔPA .

The only previous attempt to compare B/P sizes to bar sizes for a sample of galaxies is that of Lütticke et al.

¹⁰ P = probability of an r value this high or higher under the null hypothesis of no true correlation.

(2000b), who measured various structures in near-IR images of edge-on galaxies. For six galaxies where there was a clear peanut-shaped bulge and a shelf in the mid-plane surface-brightness profile (suggesting a bar), they measured both “BPL” (the box/peanut length) and “BAL” (the bar length). Since the latter was measured at the point where the bar excess appeared to merge with the outer exponential disc, it probably corresponds (approximately) to our L_{bar} . Inverting their BAL/BPL measurements to get an equivalent to $R_{\text{box}}/L_{\text{bar}}$ yields a median value of 0.38 and a mean of 0.38 ± 0.06 . This is essentially identical to our findings when we use L_{bar} to define the bar size, and is a nice confirmation of the idea that our measurement of R_{box} in moderately inclined galaxies does indeed map to measurements of the off-plane structures of edge-on galaxies.

The mean value and range of relative B/P sizes in our sample is also in very good agreement with the predictions from simulations. For the three simulations we present in this paper, we find (using the same measurement techniques) $R_{\text{box}}/L_{\text{bar}} = 0.40$ for runs A and B and 0.29 for run C. Similarly, Lütticke et al. (2000b) reported a relative size of 0.40 from their edge-on analysis of an N -body simulation originally produced by Pfenniger & Friedli (1991). And Athanasoulas & Misiriotis (2002) reported relative B/P sizes (their LP/L_2) of 0.3–0.6 for a set of three N -body simulations, sampled at two different times each. We can also use the observational results as tests for future theoretical studies: simulations which produce relative B/P sizes > 0.6 will probably not be good matches to the majority of barred galaxies, though we cannot rule them out as possible extreme cases.

Finally, the fact that B/P bulges typically span less than half the length of the bar helps answer objections which have sometimes been raised to the idea that B/P bulges in edge-on galaxies are due to bars. For example, Kormendy & Kennicutt (2004) argued that evidence for flat (outer) bars in a few edge-on galaxies such as NGC 4762, and the fact that boxy bulges have smaller sizes than bars, presented “a serious collision between simulations and observations.” But in reality there is no such collision: both theory and observations agree that only the inner parts of bars become vertically thickened.

6 DISCUSSION

6.1 Thin Bars: Identifying Galaxies Where the Bar Has Not Buckled

We have shown that the majority of bars in S0–Sb galaxies probably have B/P structures, which is consistent with the analysis of edge-on galaxies by Lütticke et al. (2000a). Is this true for *all* bars? The question of whether *some* bars are indeed flat, without any B/P structure, is an interesting one. N -body simulations generally show that bars undergo a vertical buckling instability and form B/P structures rather soon (within 1 or 2 Gyr) after the bar itself forms, and that these structures then persist as long as the bar does; thus, a barred galaxy without a B/P structure could be an indication of a very young, recently formed bar. Alternately, it may be possible to suppress buckling in some galaxies. The buckling instability results from a bar-driven increase in the in-plane stellar velocity dispersion, which leads to a large

Table 3. B/P and Bar Measurements

| Name (1) | $a(B_4)$ (2) | R_{box} (3) | PA_{box} (4) | L_{bar} (5) | PA (6) | f_{box} (7) |
|----------------|-----------------|-------------------------|--------------------------|-------------------------|-----------|-------------------------|
| Local Sample | | | | | | |
| NGC 1022 | 6.5,9.9 | 8.3 | 140.0 | 19.0 | 22.0 | 0.36 |
| NGC 2712 | 11.0,12.0 | 11.0 | 6.8 | 22.0 | 24.0 | 0.35 |
| NGC 2962 | 11.0,17.0 | 16.8 | 179.0 | 29.0 | 43.0 | 0.36 |
| NGC 3031 | 94.0,108.0 | 97.0 | 149.9 | 130.0 | 210.0 | 0.45 |
| NGC 3185 | 15.0,19.0 | 16.0 | 125.3 | 31.0 | 32.0 | 0.47 |
| NGC 3368 | 34.0,42.0 | 38.0 | 140.7 | 61.0 | 75.0 | 0.42 |
| NGC 3626 | 6.3,12.0 | 11.5 | 162.6 | 20.0 | 26.0 | 0.44 |
| NGC 3729 | 11.0,12.0 | 8.8 | 16.4 | 23.0 | 26.0 | 0.31 |
| NGC 3941 | 6.7,8.4 | 12.5 | 5.8 | 21.0 | 32.0 | 0.35 |
| NGC 4037 | 9.2,12.0 | 8.7 | 11.7 | 27.0 | 33.0 | 0.26 |
| NGC 4102 | 6.0,7.5 | 5.1 | 50.7 | 10.0 | 15.0 | 0.29 |
| NGC 4143 | 6.1,7.8 | 10.4 | 146.8 | 17.0 | 28.0 | 0.33 |
| NGC 4319 | 5.3,10.0 | 7.3 | 152.3 | 15.0 | 17.0 | 0.43 |
| NGC 4340 | 27.0,30.0 | 21.0 | 85.9 | 39.0 | 48.0 | 0.27 |
| NGC 4386 | 9.6,13.0 | 15.0 | 137.9 | 25.0 | 36.0 | 0.41 |
| NGC 4699 | 3.6,4.7 | 6.5 | 45.9 | 13.0 | 16.0 | 0.40 |
| NGC 4725 | 40.0,64.0 | 63.0 | 38.5 | 118.0 | 125.0 | 0.50 |
| NGC 4995 | 7.1,10.0 | 8.2 | 64.6 | 16.0 | 19.0 | 0.34 |
| NGC 5377 | 21.0,39.0 | 26.5 | 37.5 | 58.0 | 67.0 | 0.37 |
| NGC 5740 | 5.2,9.5 | 7.4 | 158.2 | 12.0 | 14.0 | 0.36 |
| NGC 5750 | 14.0,17.0 | 10.5 | 77.9 | 20.0 | 22.0 | 0.28 |
| NGC 5806 | 10.0,20.0 | 16.5 | 169.8 | 37.0 | 38.0 | 0.43 |
| NGC 7743 | 13.0,25.0 | 21.5 | 96.6 | 31.0 | 37.0 | 0.58 |
| IC 1067 | 5.1,8.1 | 8.5 | 142.0 | 19.0 | 19.0 | 0.43 |
| Other Galaxies | | | | | | |
| NGC 1023 | 22.0,35.0 | 28.0 | 79.7 | 40.0 | 58.0 | 0.41 |
| NGC 1808 | 34.0,50.0 | 38.0 | 140.7 | 80.0 | 114.0 | 0.33 |
| NGC 2442 | 25.0,38.0 | 29.0 | 55.8 | 57.0 | 65.0 | 0.41 |
| NGC 3627 | 17.0,32.0 | 18.0 | 165.9 | 41.0 | 53.0 | 0.32 |
| NGC 3992 | 30.0,38.0 | 25.0 | 57.0 | 54.0 | 57.0 | 0.35 |
| NGC 4123 | 16.0,27.0 | 15.0 | 112.0 | 48.0 | 50.0 | 0.29 |
| NGC 4293 | 17.0,28.0 | 17.0 | 80.0 | 61.0 | 65.0 | 0.27 |
| NGC 4535 | 16.0,19.0 | 17.0 | 31.0 | 37.0 | 40.0 | 0.41 |
| NGC 5641 | 9.0,13.0 | 11.0 | 159.0 | 23.0 | 24.0 | 0.44 |
| NGC 6384 | 8.4,16.0 | 13.0 | 36.5 | 22.0 | 27.0 | 0.48 |
| IC 5240 | 13.0,27.0 | 17.0 | 92.6 | 36.0 | 36.0 | 0.46 |

Radial lengths and position angles of B/P structures and overall bar sizes; all lengths are in arc seconds. (1) Galaxy name. (2) Semi-major axes defined by ellipse-fit B_4 values: first number = minimum B_4 (= maximum boxyness of isophotes); second = first zero-crossing of B_4 outside. (3) Direct measurement of boxy region size on the image. (4) Position angle of boxy region. (5) Bar semi-major axis. (6) Position angle of bar. (7) Size of boxy region as fraction of full bar length = $R_{\text{box}}/L_{\text{bar}}$ (deprojected).

anisotropy in the dispersion (Araki 1985; Fridman & Polyachenko 1984; Merritt & Sellwood 1994). The instability can be suppressed, however, if the disc is already vertically hot. The presence of significant gas can also suppress buckling, at least in simulations (Berentzen et al. 1998; Debattista et al. 2006), while Sotnikova & Rodionov (2005) suggest that the presence of a compact, massive, spheroidal bulge could also work. Finally, the alternative, resonance-trapping mechanism suggested by Quillen (2002) predicts that bars should thicken vertically as soon as they form: in this scenario, *all* bars should have a B/P structure: “...barred galaxies should never be found without boxy/peanut-shaped bulges”.

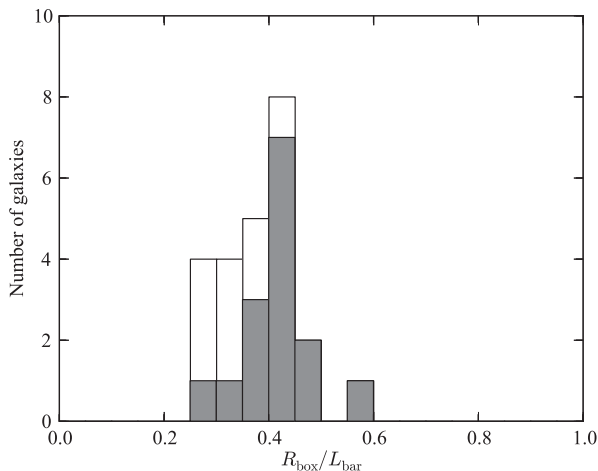


Figure 12. Distribution of relative sizes (radius of B/P structure R_{box} relative to bar radius L_{bar}) for the local sample. Open bars: all 24 galaxies with detected boxy-bar signatures. Grey bars: restricted to the 17 galaxies with (deprojected) angle between bar and disc major axis $\leq 45^\circ$, which maximizes detection of the B/P structure.

As we have seen, the higher the inclination, the easier it is to detect the projected signature of a B/P structure – if the bar’s orientation is not too far away from the major axis of the galaxy (e.g., Figure 5). Once the inclination becomes too high (say, $i > 70^\circ$), however, it becomes increasingly hard to directly detect the presence of a bar in the galaxy disc plane. This is why it is difficult to clearly identify cases in *edge-on* discs where a bar has formed but has *not* buckled or otherwise thickened to form a B/P structure.

The best places to look, then, would be barred galaxies with moderately high inclinations – e.g., $i \sim 45\text{--}70^\circ$ – where the bar’s (deprojected) position angle is within $\sim 45^\circ$ of the major axis. If such galaxies do *not* show indications of the boxy-bar morphology, then they are good candidates for systems with completely flat bars.

In Section 4.2, we used a slightly more generous limit of $i = 40^\circ$ and $\Delta\text{PA} < 45$ when attempting to determine the frequency of the boxy-bar morphology. Of the 22 galaxies in our local sample meeting those criteria, we found 14 with at least a boxy interior (and 13 with clear spurs in addition), which leaves eight galaxies which might lack a B/P structure. If we increase the inclination limit to 45° , then there are six out of 16 galaxies which do not have good evidence for a projected B/P structure. Most of these are galaxies with very weak, oval bars and/or evidence for rather luminous bulges, so that it is more difficult to discern clear morphological features belonging to just the bars.¹¹ However, there are two systems with very strong, narrow bars and no evidence for large bulges which are our best candidates for barred galaxies without B/P structures.

Figure 13 shows these two galaxies: NGC 3049 and IC 676. They have inclinations of $\approx 51^\circ$ and 47° , respectively, and bars offset from the disc major axis with (deprojected) angles of $\sim 8^\circ$ and 41° , respectively. Given these orientations and the strength of the bars, we should be able

to see the box+spurs pattern quite clearly. But as the figure shows, there is no indication of this: the bars appear to be uniformly narrow. (A possible hint of narrow, offset spurs is visible in NGC 3049 at a radius of $\sim 15''$; however, the apparent offset is in the *wrong* direction: towards the line of nodes rather than away from it.) Since there is no evidence for significant bulges in these galaxies – indeed, they seem to have little or no bulge at all – we can rule out the possibility of a boxy zone being lost within the isophotes of an elliptical bulge.

For comparison, Figure 14 shows two stages from the one of our N -body simulations: before the bar has buckled (top panels), and after (bottom panels). When the simulated galaxy is projected with approximately the same orientations as NGC 3049 and IC 676 (middle and right-hand panels), the top panels – showing the simulation *before* bar-buckling – are clearly better matches to the galaxies in question. This agreement suggests that the bars in NGC 3049 and IC 676 have *not* vertically buckled.

The extremely narrow bars, along with the absence of any sizeable bulge in these galaxies, are also reminiscent of the nearly face-on ($i = 21^\circ$) SBd galaxy NGC 600, where Méndez-Abreu et al. (2008) failed to find any kinematic signature of a B/P structure.

Very roughly speaking, then, we can put a lower limit on the frequency of vertically thin bars at $13_{-6}^{+11}\%$. If we include all of the uncertain cases – galaxies with weak, oval bars or large bulges – then the upper limit would be $38_{-11}^{+13}\%$. In any case, the existence of thin bars can be used to help constrain models of B/P structure formation. The resonance trapping model of Quillen (2002), which implies that *all* bars should have B/P structures, evidently cannot be a very common mechanism. The ability to identify both buckled and non-buckled bars in larger samples, combined with comparisons of galaxy properties between buckled and non-buckled bars, will help determine whether buckling is actually suppressed on long timescales (e.g., when significant amounts of gas are present, or when discs are vertically hot), or whether galaxies like NGC 3049 and IC 676 have simply formed their bars recently enough that buckling has not yet taken place.

6.2 Things (Mostly) Not Seen: Pinching of the Boxy Zone

Although the matching of projected bar structure between N -body simulations and actual galaxies with similar orientations can be quite good, there is a feature of the projected simulations which is rarely seen in real galaxies with moderate inclinations. Specifically, the isophotes of the boxy zone often show “pinching” in the simulations viewed at moderate inclinations (e.g., the $\Delta\text{PA} = 0^\circ$ and 30° views at $i = 60^\circ$ in Figure 5). The cause of the pinched isophotes in the simulations is not hard to divine: it is the signature of a strong peanut structure, something which manifests more clearly as an “X” shape when the simulation is seen edge-on.

Why do real galaxies not show such strong pinching when viewed at moderate inclinations? The most obvious cause is probably the presence of extra stellar structure in the inner regions of these galaxies. A compact bulge – or even a compact nuclear or inner disc (e.g., Erwin et al. 2003) – will contribute rounder isophotes in the central few hundred parsecs, and the resulting summed isophotes will tend to

¹¹ NGC 4941 has slightly boxy isophotes, but no clear spurs.

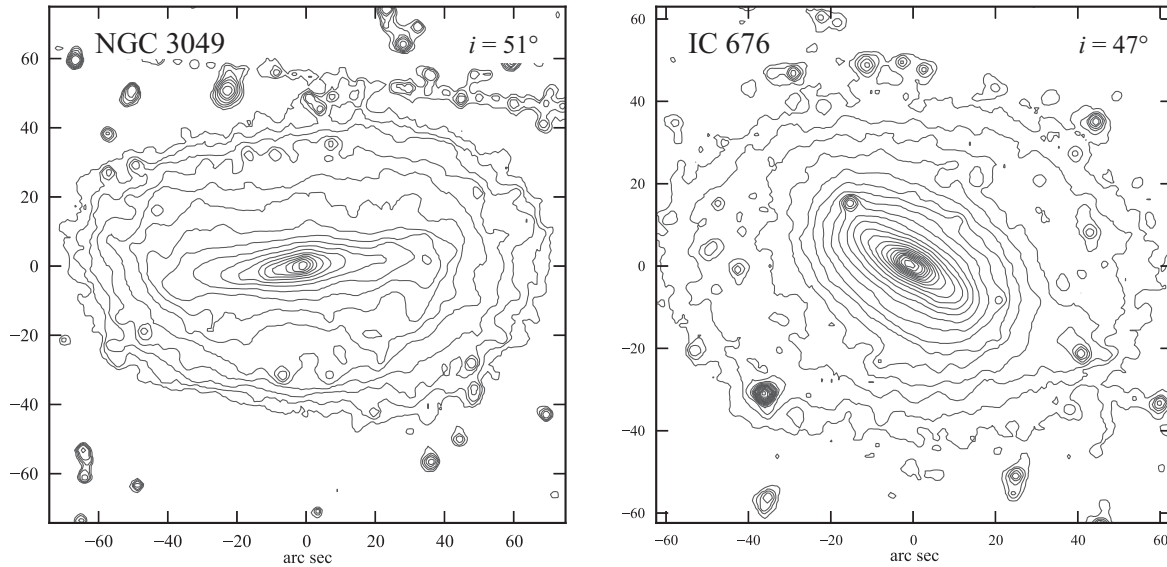


Figure 13. Left: Logarithmically scaled isophotes for SBab galaxy NGC 3049 (inclination $i \approx 51^\circ$), using *Spitzer* IRAC1 image from the SINGS project (Kennicutt et al. 2003), via NED. **Right:** Isophotes for the SB0 galaxy IC 676 ($i \approx 47^\circ$), using archival IRAC1 image from S⁴G (Sheth et al. 2010). Both images have been rotated to place the disc major axes horizontal. Despite the relatively high inclinations and favorable bar orientations (deprojected bar-disc $\Delta PA = 8^\circ$ for NGC 3049, 41° for IC 676), there is little or no sign of the box+spurs morphology in either galaxy, suggesting their bars may not have buckled. Compare with Figure 14.

smooth out the pinching. Since our N -body simulations were prepared using pure discs (no pre-existing bulges) and do not include any gas or star formation, this lack of extra, rounder components in the central regions is not surprising.

Nonetheless, we can identify *some* real galaxies where boxy zone shows pinching. Figure 15 shows two such galaxies with $i < 70^\circ$. A very slight hint of pinching can also (perhaps) be seen in the boxy zone of IC 5240’s bar (bottom right panel of Figure 2).

6.3 Using the Boxy-Bar Morphology to Constrain Galaxy Orientations

As we pointed out in Section 3.1, the offset spurs in the box+spurs morphology are due to misalignment between the bar position angle and the galaxy line of nodes. (If the spurs are symmetric, it means the bar and the line of nodes have the same position angle.) The projection effects which produce this also ensure that the visual misalignment between the inner boxy zone and the spurs is such that the spurs are always offset *away from* the line of nodes.

This means that it is possible to use the observed boxy-bar morphology to help distinguish, in a qualitative sense, between possible values of the galaxy major axis in cases where the latter is uncertain – e.g., because the galaxy is warped, interacting, or otherwise strongly asymmetric in its outer regions.

NGC 2712 is a galaxy in our local sample for which H I mapping by Krumm & Shane (1982) suggests a kinematic major-axis position angle of $\sim 10^\circ$, similar to that of the (bar-dominated) inner disc. Krumm & Shane noted that “beyond about $1'$, however, the optical major axis twists to a position angle $-2^\circ \dots$ This change of position angle is not clearly reflected in the velocity field, but our poor spatial resolution could hide such an effect.” The inner kinematic

position angle could be affected by the bar; on the other hand, the outer optical position angle might be the result of warping or other asymmetry in the disc. So which position angle better describes the galaxy orientation?

J -band isophotes for NGC 2712 can be seen in the upper-right panel of Figure A1. The spurs are strongly displaced in a counter-clockwise direction from the major axis of the boxy region ($PA \approx 7^\circ$, marked by red arrows). If the true line of nodes is at 10° , then this morphology is difficult to explain: the spurs should be offset only slightly, and in the clockwise direction. But if the line of nodes is instead 178° (dashed grey line), then the morphology makes sense: the boxy region is slightly tilted counter-clockwise with respect to the line of nodes, while the spurs are further offset in the same direction.

SUMMARY

We have presented evidence for a common pattern in moderately inclined barred galaxies, which we term the “boxy-bar” or “box+spurs” morphology. In this morphology, the bar is made of two regions: the interior is broad and slightly boxy in shape, while the outer part of the bar forms narrower “spurs”; these spurs are almost always offset or even rotated with respect to the major axis of the inner, boxy region.

By comparison with N -body simulations, we demonstrate that this morphology results from the simultaneous projection of the vertically thickened (“buckled”) inner part of a bar – the box/peanut (B/P) structure – and the vertically thin outer part of the bar. While such structures are often seen in edge-on galaxies as boxy or peanut-shaped bulges (if the bar is favorably aligned), we find that they

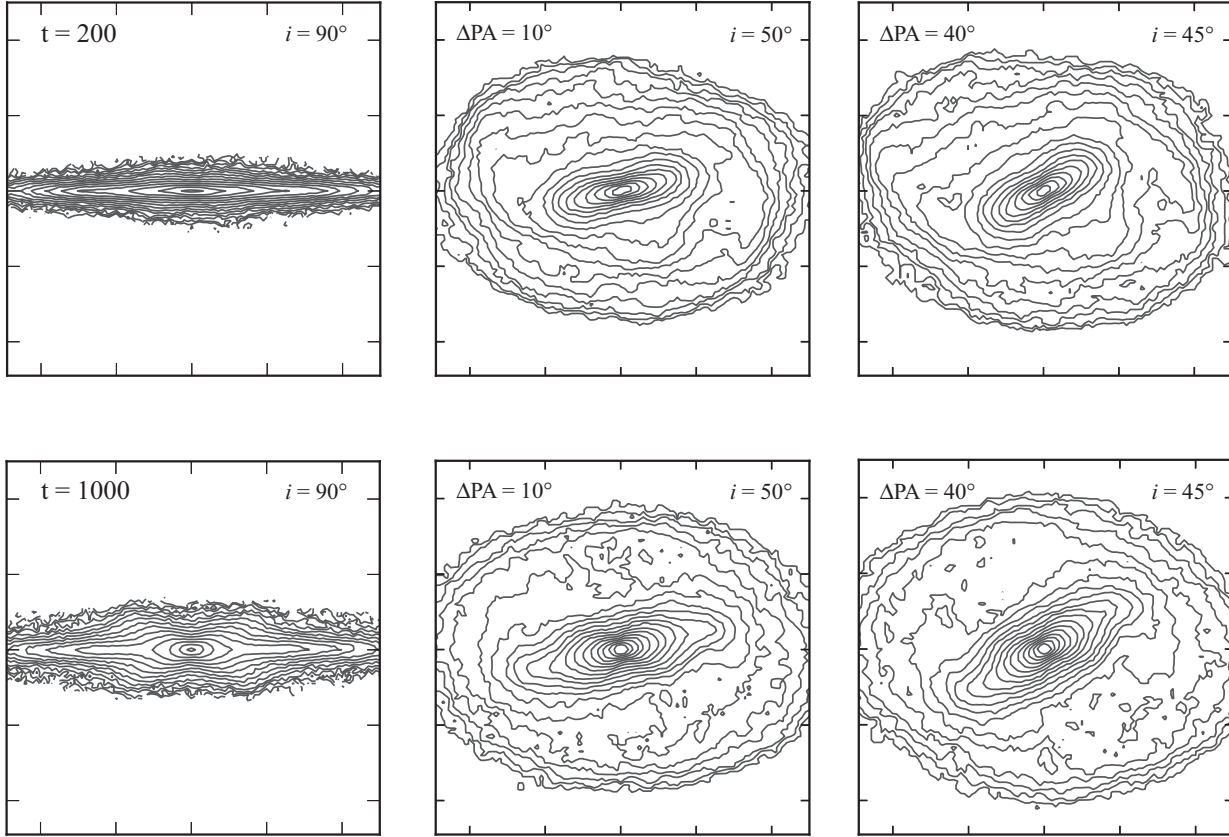


Figure 14. Logarithmically scaled isodensity contours from N -body model B, showing two snapshots: $t = 200$ (top panels), prior to bar buckling; and $t = 1000$ (bottom panels), after the bar has buckled. The left-hand panels show the edge-on ($i = 90^\circ$) view with the bar perpendicular to the line of sight, to emphasize the presence (or absence) of the box/peanut structure; the middle panels simulate observing the galaxy at an inclination of 50° , with the bar offset at $\Delta\text{PA} = 10^\circ$ (in the disc plane) from the major axis, which is horizontal; and the right-hand panels do the same but with $i = 45^\circ$ and $\Delta\text{PA} = 40^\circ$. In the later snapshot (lower panels), the bar has clearly buckled, producing strong peanut-shaped isophotes when seen edge-on (lower left) and a box+spurs morphology, with slightly offset spurs, when seen at intermediate inclination (lower middle and right). Compare with Figure 13.

can also be detected for inclinations down to $\sim 40^\circ$ – and, in exceptional cases, as low as $\sim 25\text{--}30^\circ$.

Examination of ellipse fits to galaxies (real and simulated) with boxy-bar morphologies shows that a general set of criteria using A_4 and B_4 (the $\sin 4\theta$ and $\cos 4\theta$ deviations from pure ellipticity) exist for identifying most – but not all – cases. However, we argue that ellipse fits do not provide a consistent and reliable means of measuring the *size* of the boxy zone, and recommend direct measurements on images instead.

For the latter purpose, we define a visual size measurement for the boxy zone: R_{box} . Comparison of different projections of N -body simulations shows that R_{box} does an excellent job of describing the radial extent of the B/P structure as seen in edge-on views; consequently, we are confident that measurements of R_{box} in real (moderately inclined) galaxies provides a good estimate of the extent of B/P structures.

Starting with a local sample of 78 bright S0–Sb barred galaxies with inclinations $\lesssim 65^\circ$, we find 24 galaxies showing some form of the box+spurs morphology. If we restrict ourselves to the subset of inclinations and relative position angles (between bar and disc major axis) which maximizes

detection of this morphology, we estimate that at least 2/3 of S0–Sb bars are vertically thickened in their interiors.

Using the R_{box} measurement, we find that the B/P structure in our local galaxy sample spans a range of 0.26–0.58 of the full bar length, with a mean of $R_{\text{box}}/L_{\text{bar}} = 0.38 \pm 0.08$; the latter is in excellent agreement with measurements from a set of six *edge-on* galaxies by Lütticke et al. (2000b). This is clear evidence that when bars thicken vertically, it is only the inner one- to two-thirds (typically just under half) of the bar which does so.

We note that the combination of being able to easily identify bars when galaxies are not highly inclined (e.g., $i \lesssim 75^\circ$) and the clear features of projected B/P structures when the galaxy has an inclination $\gtrsim 45^\circ$ creates a “sweet spot” for finding bars which do *not* have a B/P structure: galaxy inclination between $\sim 45^\circ$ and 70° and bar orientation $\lesssim 45^\circ$ away from the galaxy line of nodes. From our local sample, we identify NGC 3049 and IC 676 as plausible candidates for galaxies with non-buckled (uniformly thin) bars. This implies a lower limit of $\sim 13\%$ on the fraction of bars which have not buckled.

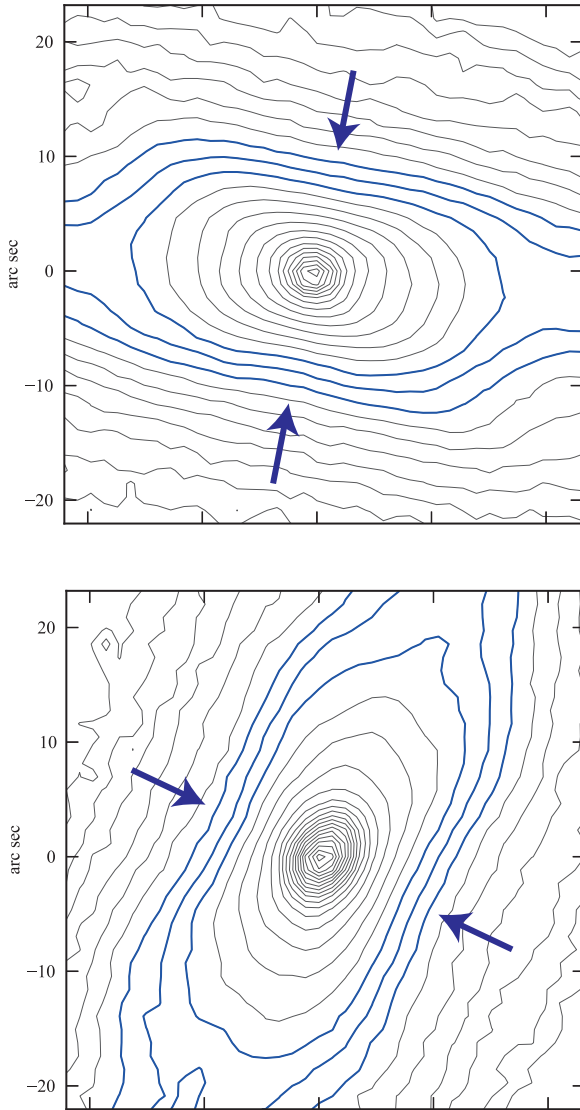


Figure 15. Log-scaled H -band isophotes for NGC 4293 (top) and NGC 7582 (bottom), showing evidence for “pinched” isophotes in the box region (blue arrows; the isophotes showing this are outlined with thicker blue lines). Both images are from Eskridge et al. (2002); N is up and E is to the left.

ACKNOWLEDGMENTS

We are happy to thank Inma Martinez-Valpuesta for helpful comments and conversations, and Ron Buta for suggesting several candidate boxy-bulge galaxies. Both of them, along with Lia Athanassoula, Alfonso Aguerri, Dimitri Gadotti, Jairo Méndez-Abreu, and Panos Patsis, read and provided numerous comments on earlier drafts, which helped improve the paper; we also thank the anonymous referee. P.E. was supported by the Deutsche Forschungsgemeinschaft through Priority Programme 1177 “Galaxy Evolution”; V.P.D. is supported by STFC Consolidated grant # ST/J001341/1.

This work is based in part on observations made with the *Spitzer* Space Telescope, obtained from the NASA/IPAC Infrared Science Archive, both of which are operated by the Jet Propulsion Laboratory, California Institute of Technol-

ogy under a contract with the National Aeronautics and Space Administration.

Funding for the creation and distribution of the SDSS Archive has been provided by the Alfred P. Sloan Foundation, the Participating Institutions, the National Aeronautics and Space Administration, the National Science Foundation, the U.S. Department of Energy, the Japanese Monbukagakusho, and the Max Planck Society. The SDSS Web site is <http://www.sdss.org/>.

The SDSS is managed by the Astrophysical Research Consortium (ARC) for the Participating Institutions. The Participating Institutions are The University of Chicago, Fermilab, the Institute for Advanced Study, the Japan Participation Group, The Johns Hopkins University, the Korean Scientist Group, Los Alamos National Laboratory, the Max-Planck-Institute for Astronomy (MPIA), the Max-Planck-Institute for Astrophysics (MPA), New Mexico State University, University of Pittsburgh, University of Portsmouth, Princeton University, the United States Naval Observatory, and the University of Washington.

Finally, this research has made extensive use of the NASA/IPAC Extragalactic Database (NED), which is operated by the Jet Propulsion Laboratory, California Institute of Technology, under contract with the National Aeronautics and Space Administration.

REFERENCES

- Abazajian K. N. et al., 2009, *ApJS*, 182, 543
- Araki S., 1985, PhD thesis, MIT
- Athanassoula E., 1992, *MNRAS*, 259, 345
- Athanassoula E., 2005a, *MNRAS*, 358, 1477
- Athanassoula E., 2005b, in Szczerba R., Stasińska G., Górny S. K. eds., *Planetary Nebulae as Astronomical Tools*. AIP Conference Proceedings, Melville, New York, 333
- Athanassoula E., Bureau M. 1999, *ApJ*, 522, 699
- Athanassoula E., Misiriotis A., 2002, *MNRAS*, 330, 35
- Athanassoula E., Beaton R. L., 2006, *MNRAS*, 370, 1499
- Beaton R. L. et al., 2007, *ApJL*, 658, L91
- Bender, R., Döbereiner S., Möllenhoff C., 1988, *A&A*, 74, 385
- Berentzen I., Heller C. H., Shlosman I., Fricke K. J., 1998, *MNRAS*, 300, 49
- Bertola F., Capaccioli M., 1977, *ApJ*, 211, 697
- Bettoni D., Galletta G., 1994, *A&A*, 281, 1
- Binggeli B., Sandage A., Tammann G. A., 1985, *AJ*, 90, 1681
- Binney J., Petrou M., 1985, *MNRAS*, 214, 449
- Blackeslee J. P. et al., 2009, *ApJ*, 694, 556
- Böker T. et al., 1999, *ApJS*, 124, 95
- Bureau M., Freeman K. C., 1999, *AJ*, 118, 126
- Bureau M., Athanassoula E., 2005, *ApJ*, 626, 159
- Bureau M., Aronica G., Athanassoula E., Dettmar R.-J., Bosma A., Freeman K. C., 2006, *MNRAS*, 370, 753
- Buta R., 1990, *ApJ*, 356, 87
- Combes F., Sanders R. H., 1981, *A&A*, 92, 163
- Combes F., Debbaesch F., Friedli D., Pfenniger D., 1990, *A&A*, 233, 82
- Chung A., Bureau M., 2004, *AJ*, 127, 3192
- Dale D. A. et al., 2009, *ApJ*, 703, 517

- de Souza R. E., Dos Anjos S., 1987, *A&AS*, 70, 465
- de Vaucouleurs G., de Vaucouleurs A., Corwin H. G., Buta R. J., Paturel G., Fouqué P., 1991, *Third Reference Catalogue of Bright Galaxies*. Springer-Verlag, New York (RC3)
- Debattista V. P., Carollo C. M., Mayer L., Moore B., 2005, *ApJ*, 628, 678
- Debattista V. P., Mayer L., Carollo C. M., Moore B., Wadsley J., Quinn T., 2006, *ApJ*, 645, 209
- Debattista V. P., Moore B., Quinn T., Kazantzidis S., Maas R., Mayer L., Read J., Stadel J., 2008, *ApJ*, 681, 1076
- Dettmar R.-J., Barteldrees A., 1990, in Jarvis B. J., Terndrup D. M., eds., *ESO/CTIO Workshop on Bulges of Galaxies*. ESO, Garching, p. 259
- Dwek E., et al., 1995, *ApJ*, 445, 716
- Erwin P., 2005, *MNRAS*, 364, 283
- Erwin P., Sparke L. S., 2003, *ApJS*, 146, 299
- Erwin P., Vega Beltán J. C., Graham A. W., Beckman J. E., 2003, *ApJ*, 597, 929
- Erwin P., Pohlen M., Beckman J. E., 2008, *AJ*, 135, 20
- Eskridge P. B., et al., 2002, *ApJS*, 143, 73
- Freedman W. L. et al., 2001, *ApJ*, 553, 47
- Fridman A. M., Polyachenko V. L., 1984, *Physics of Gravitating Systems* (New York: Springer)
- García-Barreto J. A., Moreno E., 2000, *ApJ*, 529, 832
- Gutiérrez L., Erwin P., Aladro R., Beckman J. E., 2011, *AJ*, 142, 145
- Jarvis B. J., 1986, *AJ*, 91, 65
- Jedrzejewski R. I., 1987, *MNRAS*, 226, 747
- Jungwiert B., Combes F., Axon D. J., 1997, *A&AS*, 125, 479
- Kennicutt, Jr. R. C. et al., 2003, *PASP*, 810, 928
- Kent S. M., Dame T. M., Fazio G., 1991, *ApJ*, 378, 131
- Koopmann R. A., Kenney J. D. P., 2006, *ApJS*, 162, 97
- Kormendy J., Illingworth G., 1982, *ApJ*, 256, 460
- Kormendy J., Kennicutt, Jr. R. C., 2004, *ARA&A*, 42, 603
- Knapen J. H., de Jong R. S., Stedman S., Bramich D. M., 2003, *MNRAS*, 344, 527
- Krumm N., Shane W. W., 1982, *A&A*, 116, 237
- Kuijken K., Merrifield M. R., 1995, *ApJL*, 443, L13
- Laurikainen E., Salo H., Buta R., Knapen J. H., 2011, *MNRAS*, 418, 1452
- Lütticke, R. Dettmar R.-J., Pohlen M., 2000a, *A&AS*, 145, 405
- Lütticke, R. Dettmar R.-J., Pohlen M., 2000b, *A&A*, 362, 435
- Martínez-Valpuesta I., Shlosman I., Heller C., 2006, *ApJ*, 637, 214
- Mei S. et al., 2005, *ApJ*, 625, 121
- Mei S. et al., 2007, *ApJ*, 655, 144
- Méndez-Abreu J., Corsini E. M., Debattista V. P., De Rijcke S., Aguerri J. A. L., Pizzella A., 2008, *ApJL*, 679, L73
- Merrifield M. R., Kuijken K., 1999, *A&A*, 345, L47
- Merritt D., Sellwood J. A., 1994, *ApJ*, 425, 551
- Möllenhoff C., Heidt J., 2001, *A&A*, 368, 16
- Mulchaey J. S., Regan M. W., Kundu A., 1997, *ApJS*, 110, 299
- Nilson P., 1973, *Uppsala General Catalog of Galaxies*, *Uppsala Astron. Obs. Annals*, 5, 1
- Nowak N., Thomas J., Erwin, P., Saglia R. P., Bender R., Davies R. I., 2010, *MNRAS*, 403, 646
- Pancoast A., Sajina A., Lacy M., Noriega-Crespo A., Rho J., 2010, *ApJ*, 723, 530
- Patsis P. A., Skokos C., Athanassoula E., 2002, *MNRAS*, 337, 578
- Peletier R. F. et al., 1999, *ApJS*, 125, 363
- Pfenniger D., 1985, *A&A*, 150, 112
- Pfenniger D., Friedli D., 1991, *A&A*, 252, 75
- Quillen A., 2002, *AJ*, 124, 722
- Quillen A., Kuchinski L. E., Frogel J. A., Depoy D. L., 1997, *ApJ*, 481, 179
- Raha N., Sellwood J. A., James R. A., Kahn F. D., 1992, *Nature*, 352, 411
- Rest A., van den Bosch F. C., Jaffe W., Tran H., Tsvetanov Z., Ford H. C., Davies J., Schafer J., 2001, *AJ*, 121, 2431
- Sellwood J. A., Debattista V. P., 2009, *MNRAS*, 398, 1279
- Shaw M. A., 1987, *MNRAS*, 229, 691
- Shaw M. A., Dettmar R. J., Bartledrees A., 1990, *A&A*, 240, 36
- Sheth K. et al., 2010, *PASP*, 122, 1397
- Sotnikova N. Y., Rodionov S. A., 2005, *AstL*, 31, 15
- Tonry J. L., Dressler A., Blakeslee J. P., Ajhar E. A., Fletcher A. B., Luppino G. A., Metzger M. R., Moore C. B., 2001, *ApJ*, 546, 681
- Tully R. B., Rizzi L., Shaya E. J., Courtois H. M., Makarov D. I., Jacobs B. A., 2009, *AJ*, 138, 323
- Veilleux S., Bland-Hawthorn J., Cecil G., 1999, *AJ*, 118, 2108
- Willick J. A., Courteau S., Faber S. M., Burstein D., Dekel A., Strauss M. A., 1997, *ApJS*, 109, 333
- Wilson E. B., 1927, *J. Amer. Statist. Assoc.*, 22, 209
- Wozniak H., Michel-Dansac L., 2009, *A&A*, 494, 11
- Wu W., Clayton G. C., Gordon K. D., Misselt K. A., Smith T. L., Calzetti D., 2002, *ApJS*, 143, 377
- York D. G. et al., 2000, *AJ*, 120, 1579

APPENDIX A: PLOTS AND MEASUREMENTS OF B/P STRUCTURES IN SAMPLE GALAXIES

Figure A1 presents red or near-IR galaxy isophotes for the 24 galaxies in our local sample which display the box+spurs morphology, along with visual indications of the R_{box} and L_{bar} measurements for each galaxy; the numerical values can be found in Table 3. Figure A2 does the same for six more galaxies which are not part of the local sample, taken from Table 1; another six galaxies from Table 1 can be seen in Figure 7.

A1 Image Sources

We list here the sources and photometric bands of images used in the plots of the bar regions, including those used for Figures A1 and A2. Unless otherwise noted, all *Spitzer* IRAC images were retrieved from the *Spitzer* Heritage Archive; we use the standard post-BCD image generated by the archive (0.6''/pixel scale).

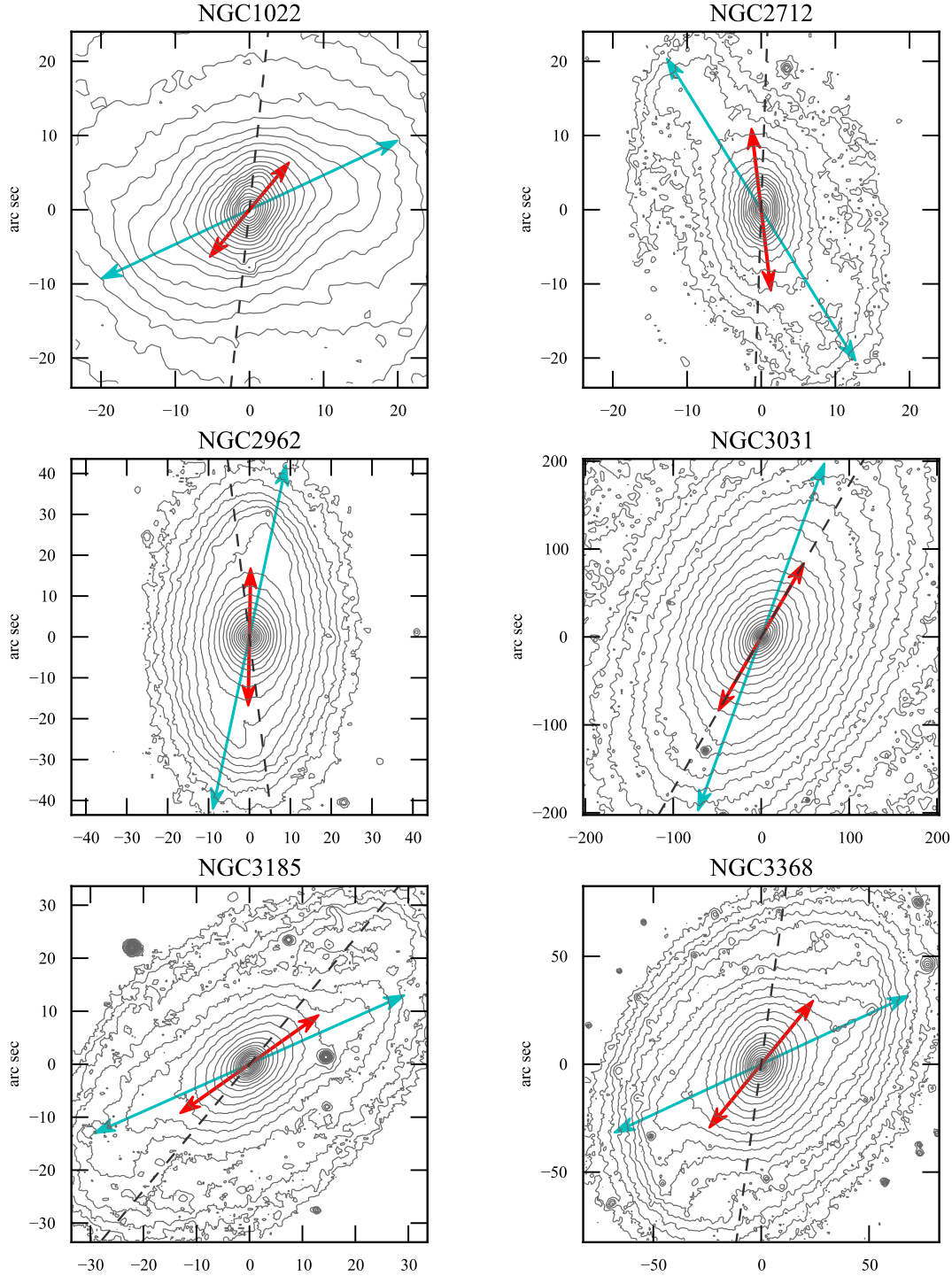


Figure A1. Plots of logarithmically scaled isophotes for galaxies in our local sample with boxy-bar morphology, focussed on the bar region. Dashed black lines indicates the disc major axis, longer (cyan) arrows indicates position angle and full length ($2 \times L_{\text{bar}}$) of the bar, and shorter (red) arrows indicate approximate position angle and full length ($2 \times R_{\text{box}}$) of the projected B/P structure. N is up and E is to the left; most isophotes are from near-IR images (see Appendix A1 for details).

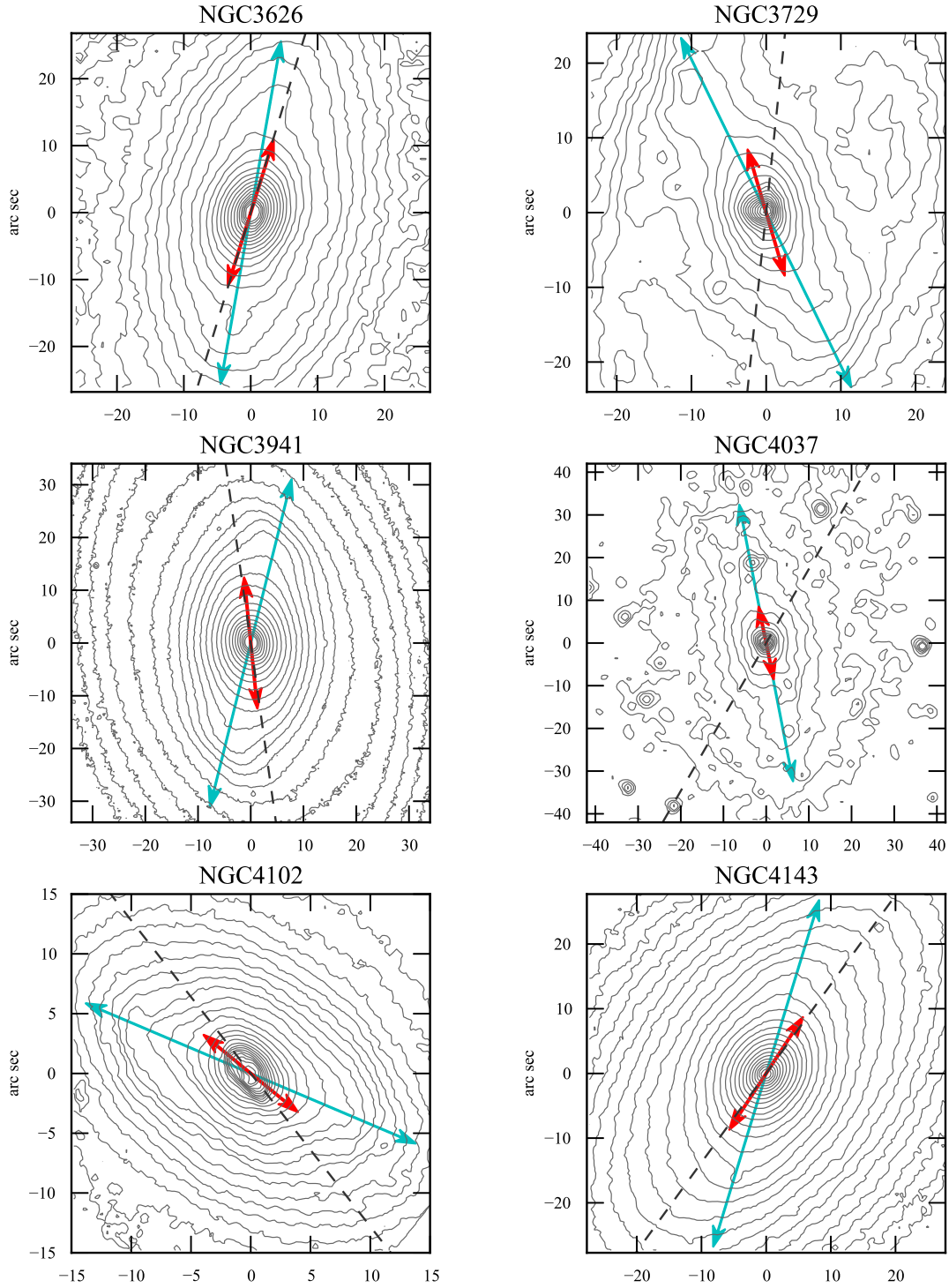


Figure A1. – continued.

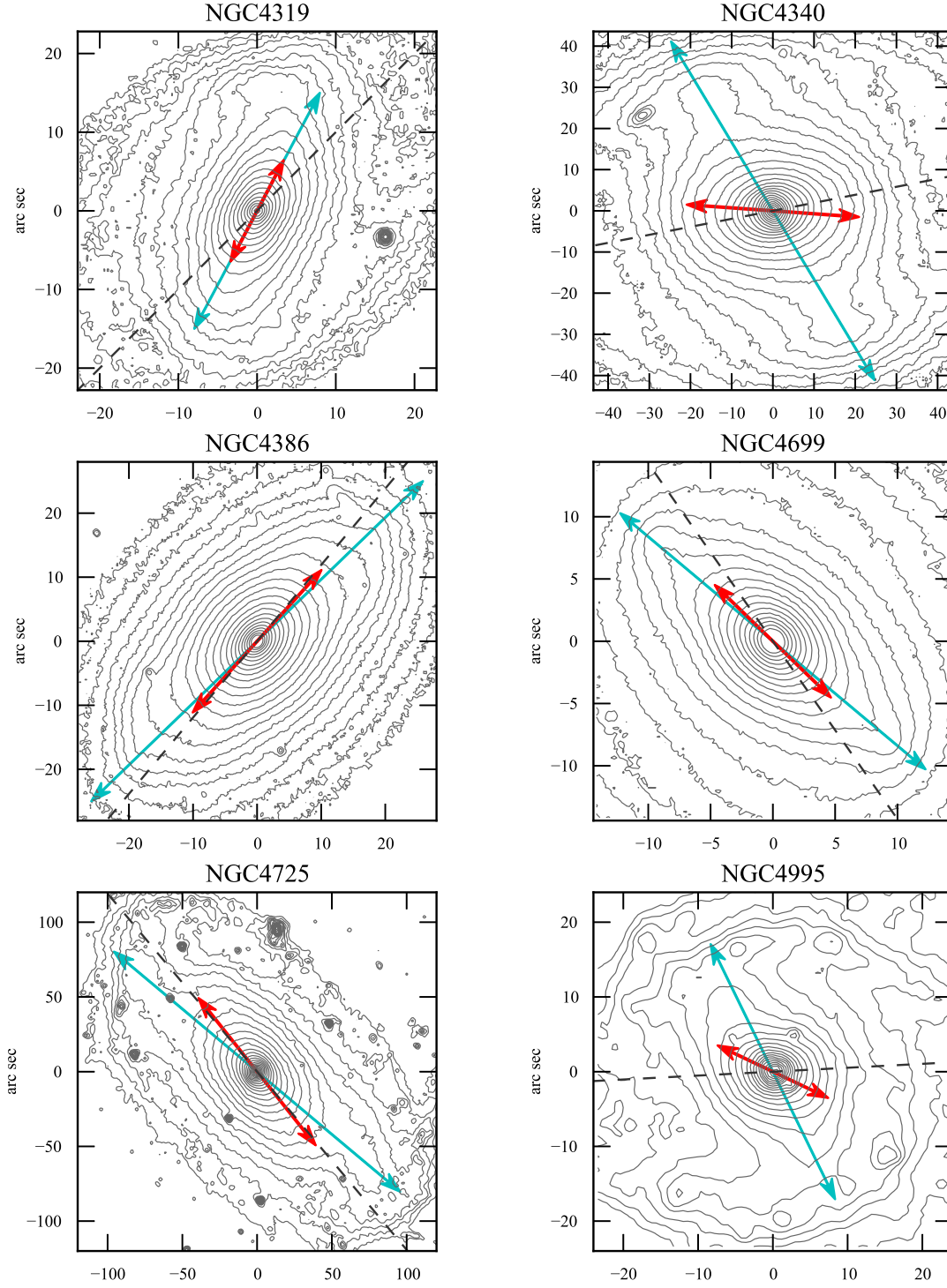


Figure A1. – continued.

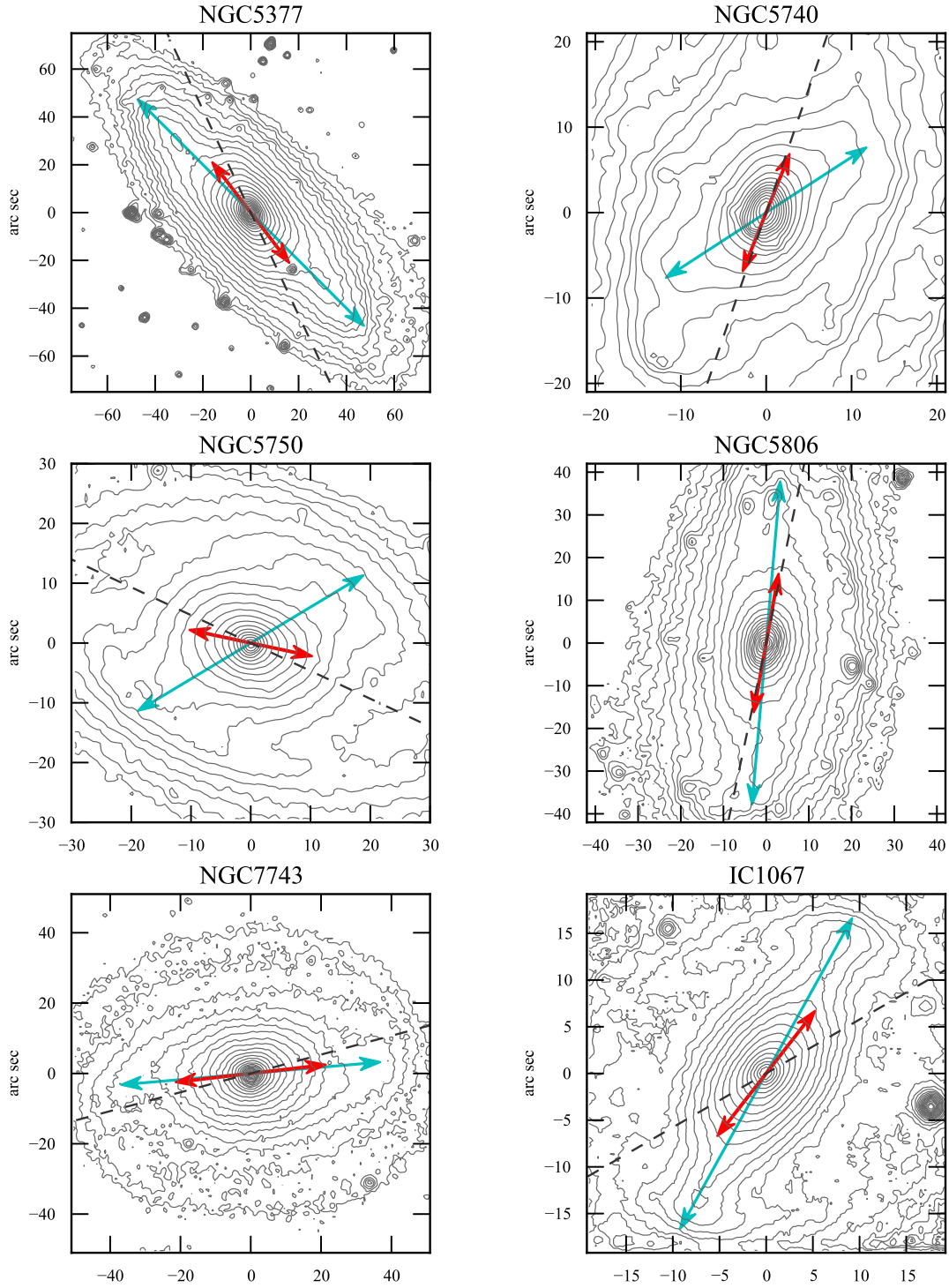


Figure A1. – continued.

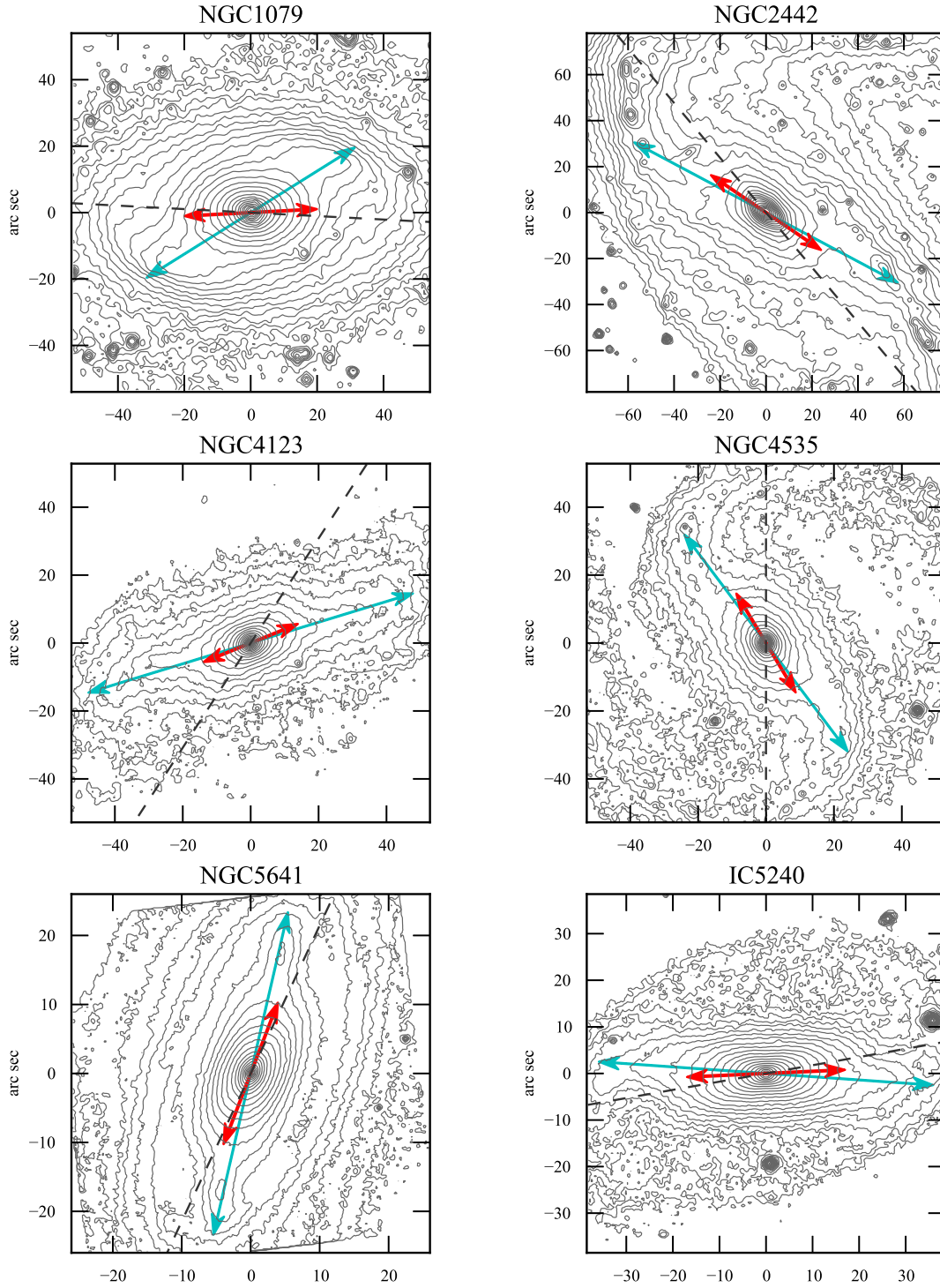


Figure A2. As for Figure A1, but now showing other galaxies with boxy-bar signatures; see Figure 7 for additional examples.

A1.1 Local Sample

NGC 1022, 4037, 4995, 5740, 5750, 5806: *Spitzer* IRAC1 images from *Spitzer* Survey of Stellar Structure in Galaxies (S⁴G; Sheth et al. 2010).

NGC 2712, 4319, 4699, IC 1067: WHT-INGRID *J*-band images.

NGC 2962: SDSS *i*-band image.

NGC 3031, 3368: *Spitzer* IRAC1 images from Dale et al. (2009), via NED.

NGC 3185: WHT-INGRID *H*-band image.

NGC 3626: *K*-band image from Möllenhoff & Heidt (2001), via NED.

NGC 3729: *Spitzer* IRAC1 image (Program ID = 61009, PI = W. Freedman).

NGC 3941, 4386: WIYN *R*-band images from Erwin & Sparke (2003).

NGC 4102: *HST* NICMOS3 F160W image from Böker et al. (1999), via NED.

NGC 4143, 4340: SDSS *r*-band image.

NGC 4725: *Spitzer* IRAC1 image from SINGS (Kennicutt et al. 2003), via NED.

NGC 5377: *Spitzer* IRAC1 image (Program ID = 69, PI = G. Fazio).

NGC 7743: *Spitzer* IRAC1 image (Program ID = 40936, PI = G. Rieke).

A1.2 Other Galaxies

NGC 1023: *J*-band image from Möllenhoff & Heidt (2001), via NED.

NGC 1808, 4293: *H*-band image from OSU Bright Spiral Galaxy Survey (Eskridge et al. 2002), via NED.

NGC 2442: *Spitzer* IRAC1 image from Pancoast et al. (2010), via NED.

NGC 3627: *Spitzer* IRAC1 image from SINGS (Kennicutt et al. 2003), via NED.

NGC 3992: *Spitzer* IRAC1 image (Program ID = 80025, PI = L. van Zee).

NGC 4123, 4535, 6384: *K*-band image from Knapen et al. (2003), via NED.

NGC 5641: *HST* NICMOS3 F160W image from Böker et al. (1999), via NED.

IC 5240: *K*-band image from Mulchaey et al. (1997), via NED.